

Archive-Mining the Galaxy Cluster Kinematic Lensing

Master's Thesis Defense

Jiyun Di

Department of Physics and Astronomy
Stony Brook University

Thursday, May 16, 2024 09:00 New York Time



Stony Brook
University

Archive-Mining the Galaxy Cluster Kinematic Lensing

Outlines

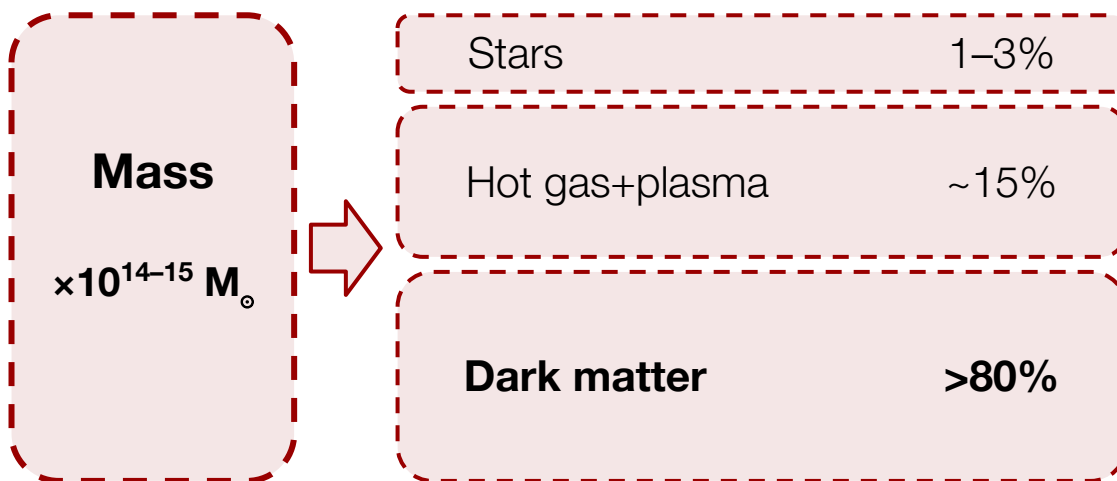
- 1. Introduction**
- 2. Kinematic Lensing**
- 3. Kinematic Lensing on “Weighing the Giants”
Galaxy Clusters with Keck/DEIMOS**



Stony Brook
University

Cluster of Galaxies

- $\times 100\text{--}1000$ galaxies
- Locates at nodes of large-scale structure webs
- Largest gravitationally-bounded structures in the Universe



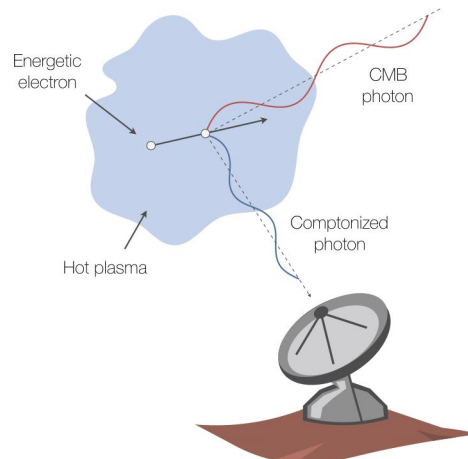
JWST/NIRCam image of galaxy cluster
SMACS 0723 at $z \sim 0.3$

<https://www.nasa.gov/image-article/nasas-webb-delivers-deepest-infrared-image-of-universe-yet/>

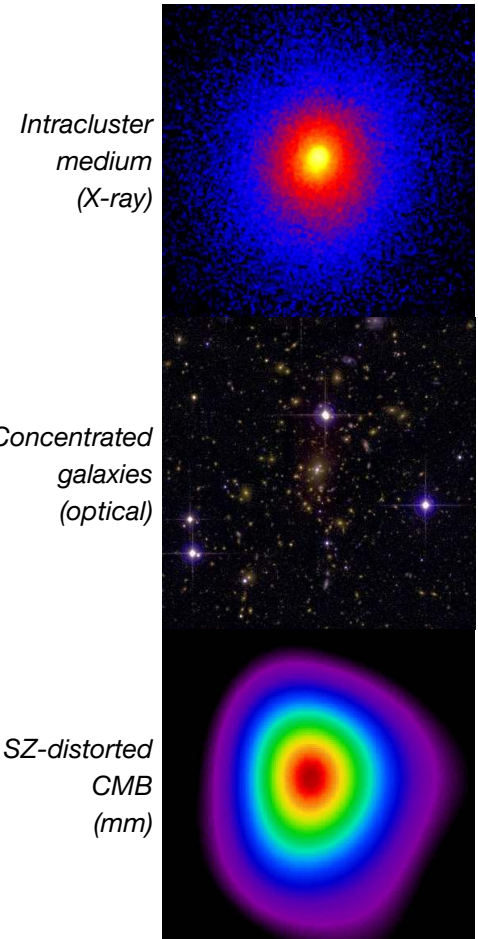
Cluster of Galaxies

Detection

- **X-ray** — emission from intracluster medium (ICM)
- **Optical** — over-densities of galaxies at similar z
- **Millimeter-wave** — cosmic microwave background (CMB) distortion, according to [Sunyaev-Zel'dovich effect](#).



Mroczkowski et al. 2019



Allen et al. 2011

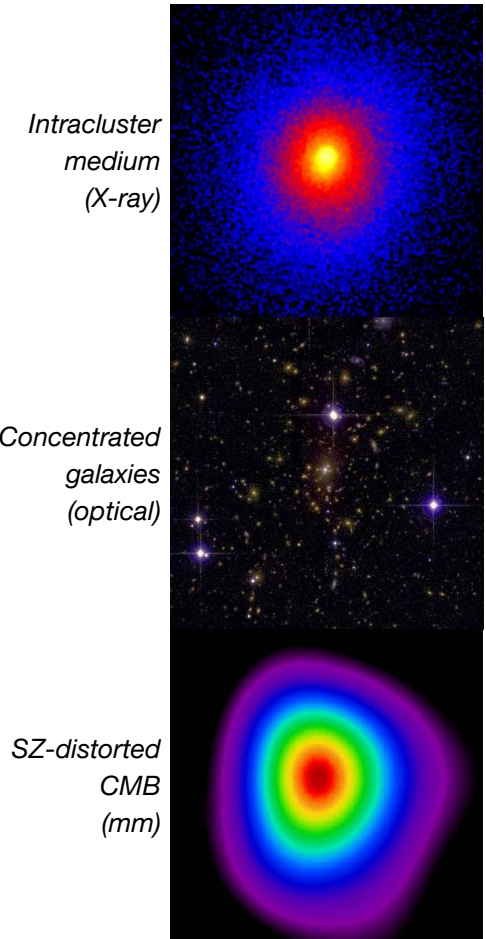
Cluster of Galaxies

Detection

- **X-ray** — emission from intracluster medium (ICM)
- **Optical** — over-densities of galaxies at similar z
- **Millimeter-wave** — cosmic microwave background (CMB) distortion, according to **Sunyaev-Zel'dovich effect**.

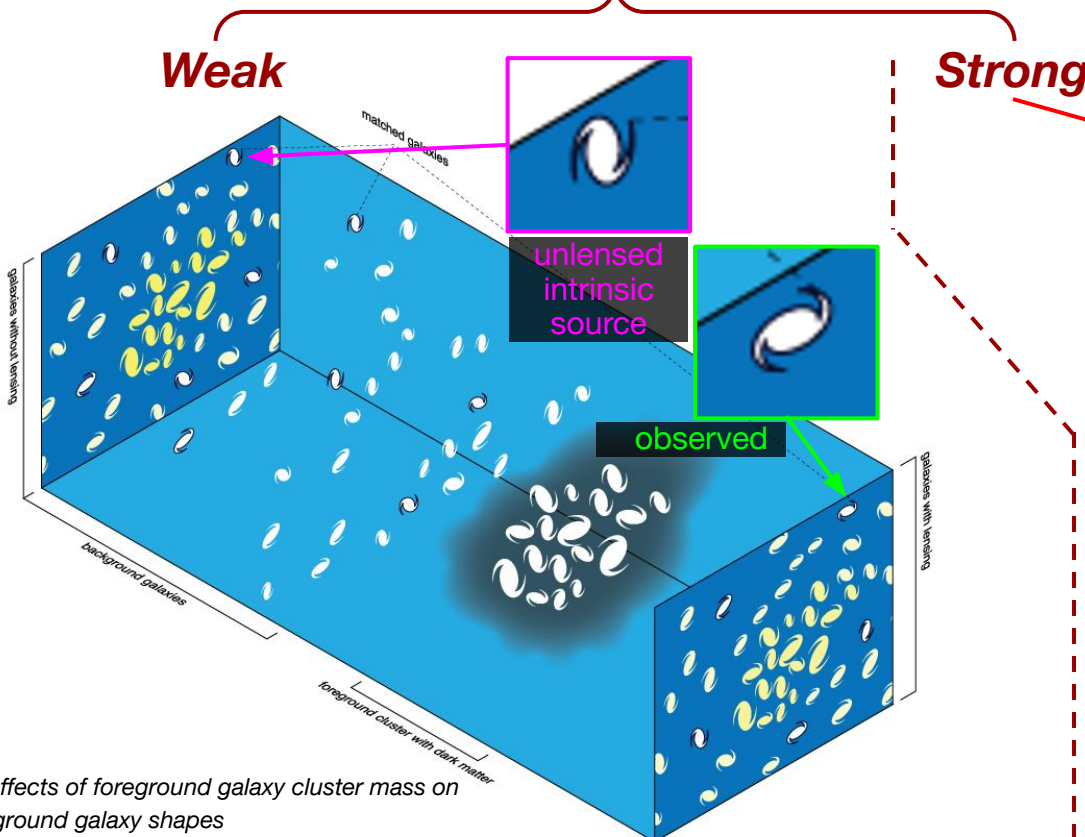
Cosmology

- Large masses
- **Gravitational Lensing** — Tightly relates the dark matter (DM) and cluster mass



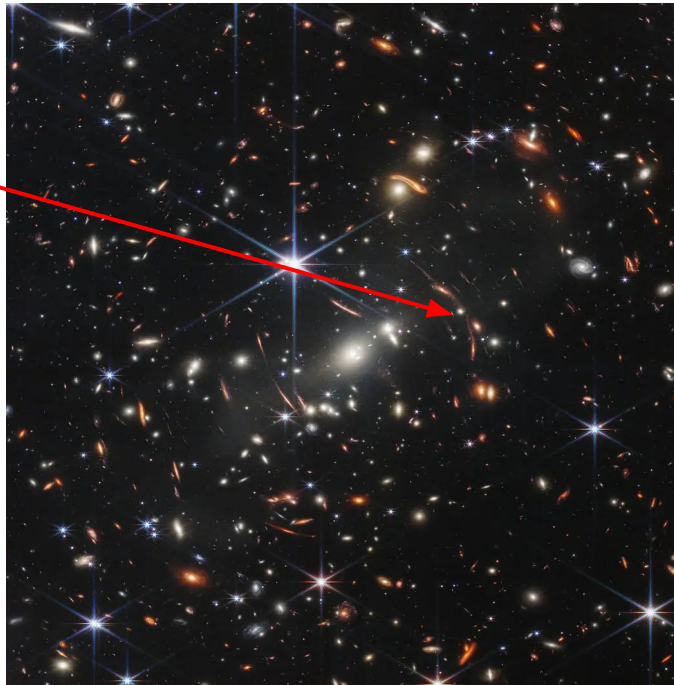
Allen et al. 2011

Gravitational Lensing



The effects of foreground galaxy cluster mass on background galaxy shapes

https://en.wikipedia.org/wiki/Weak_gravitational_lensing#Weak_lensing_by_clusters_of_galaxies

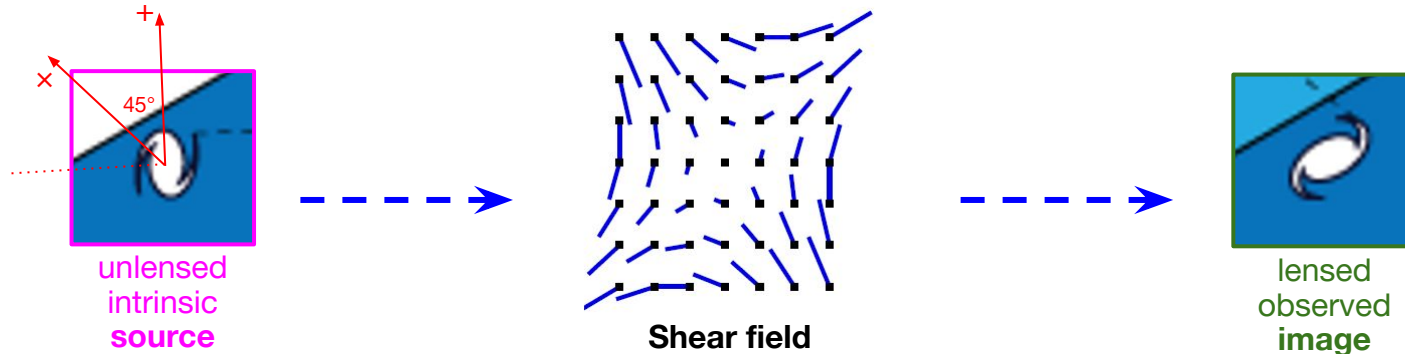


JWST/NIRCam image of galaxy cluster
SMACS 0723 at $z \sim 0.3$

<https://www.nasa.gov/image-article/nasas-webb-delivers-deepest-infrared-image-of-universe-yet/>

Weak Lensing

To measure weak shear



$$\epsilon_{\text{int}} = \epsilon_{\text{int},+} + i\epsilon_{\text{int},\times}$$

(ellipticity, in complex form)

$$\gamma = \gamma_+ + i\gamma_\times$$

$$\epsilon_{\text{obs}} = \epsilon_{\text{obs},+} + i\epsilon_{\text{obs},\times}$$

$$\boxed{\gamma + \epsilon_{\text{int}} = \epsilon_{\text{obs}}}$$

+ the component aligned with the major axis of the galaxy
× the component rotated by 45° relative to +.

Weak Lensing

To measure weak shear

Traditionally people assume a mean intrinsic shape = round

- Take **average of shears** $\langle \gamma \rangle$
- Weak-lensing cosmological constraints, shear-shear correlation, ...

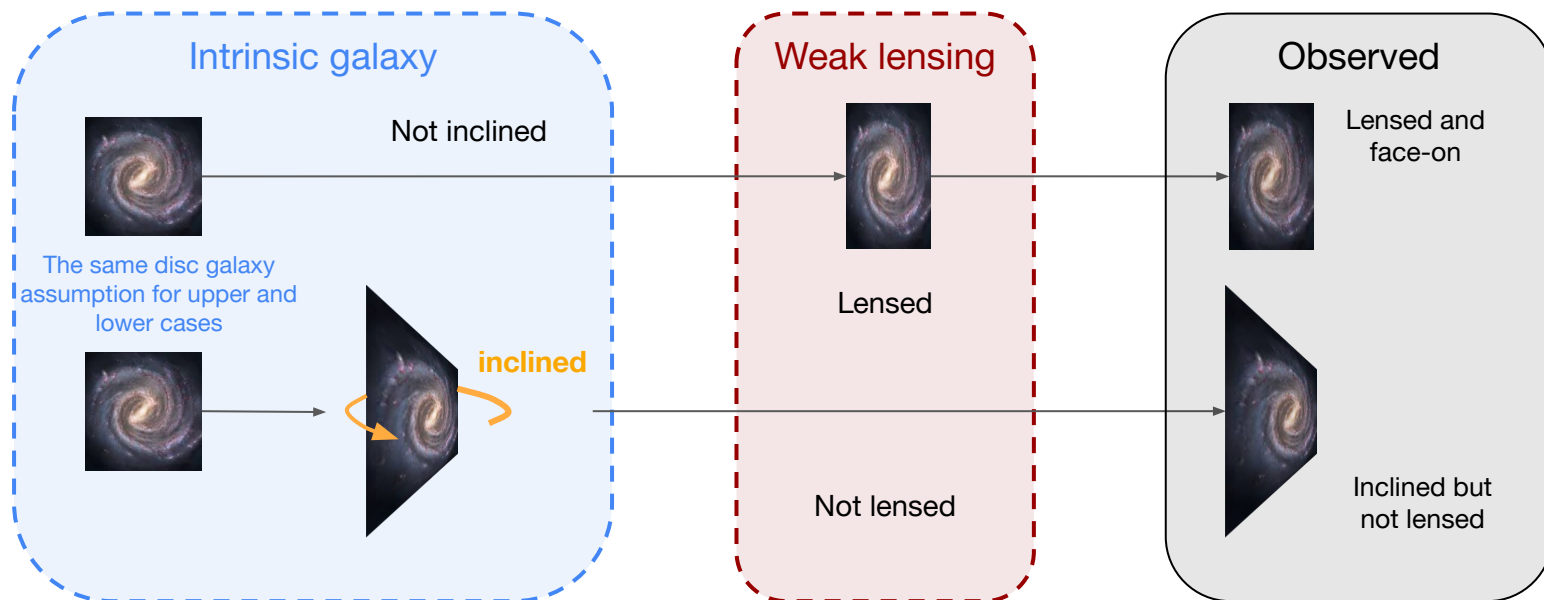
$$\gamma + \epsilon_{\text{int}} = \epsilon_{\text{obs}}$$

$$\langle \epsilon_{\text{int}} \rangle = 0$$

$$\langle \epsilon_{\text{obs}} \rangle = \gamma$$

Weak Lensing

To measure weak shear



$$\langle \epsilon_{\text{obs}} \rangle = \gamma$$

Weak Lensing - Shape Noise

To measure weak shear

Traditionally people assume a mean intrinsic shape = round

- Take **average of shears** $\langle \gamma \rangle$
- Weak-lensing cosmological constraints, shear-shear correlation, ...

Shape noise can be as high as

$$\sigma_\epsilon \sim 26\% \text{ (from LSST results),}$$

This is the maximal potential of photometry, unluckily.

$$\gamma + \epsilon_{\text{int}} = \epsilon_{\text{obs}}$$

$$\langle \epsilon_{\text{int}} \rangle = 0$$

with σ_ϵ

$$\langle \epsilon_{\text{obs}} \rangle = \gamma$$

Weak Lensing - *Shape Noise*

Better to find:

- **Intrinsic shape** (ϵ_{int}) of source galaxy
- **Resolve individual shears** γ

$$\gamma + \epsilon_{\text{int}} = \epsilon_{\text{obs}}$$

Other magics than normal photometric imaging?

— “*Kinematic Lensing*”.

Kinematic Lensing (*KL*)

An approach that utilizes both **imaging galaxy shape information** and **kinematics from slit-spectroscopy** for breaking the degeneracy between intrinsic shape and weak-lensing shear

(Huff et al. 2013)

Kinematic Lensing (*KL*)

Galaxy **spectra** → Light-of-sight rotational velocity

Tully-Fisher scaling relation → Rotational velocity

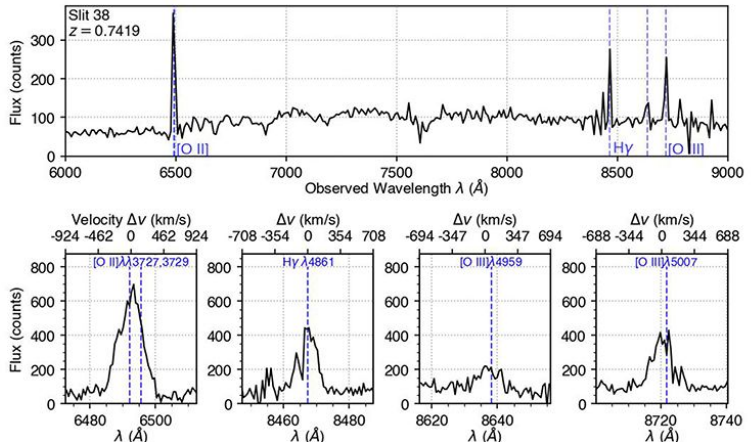


Galaxy inclination
(intrinsic shape)

(Huff et al. 2013)

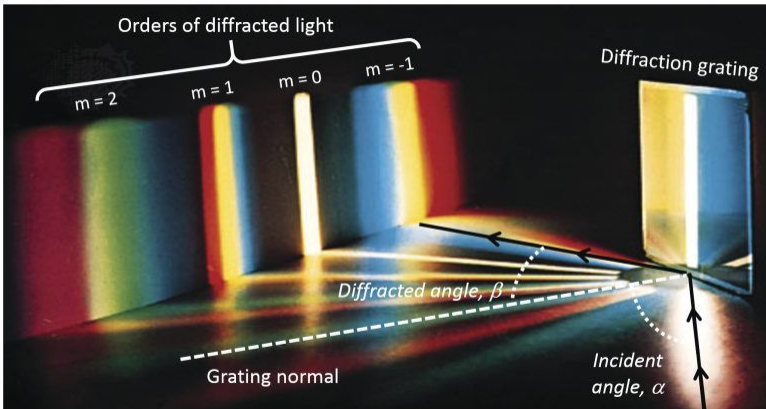
Galaxy Spectroscopy

- Spectra \longleftrightarrow Kinematic information
- Absorption and emission features on spectrum
- With templates, we'll know
 - Redshift, Galaxy type, Chemical composition



Broad and zoomed 1D spectra Slit 38

Thesis Figure



Polychromatic light diffracted from a grating

<https://www.newport.com/n/diffraction-grating-physics>

Galaxy Spectroscopy

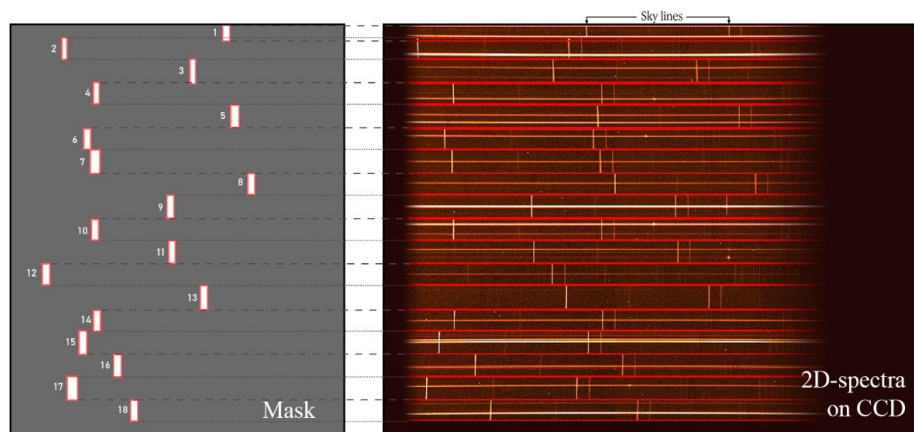
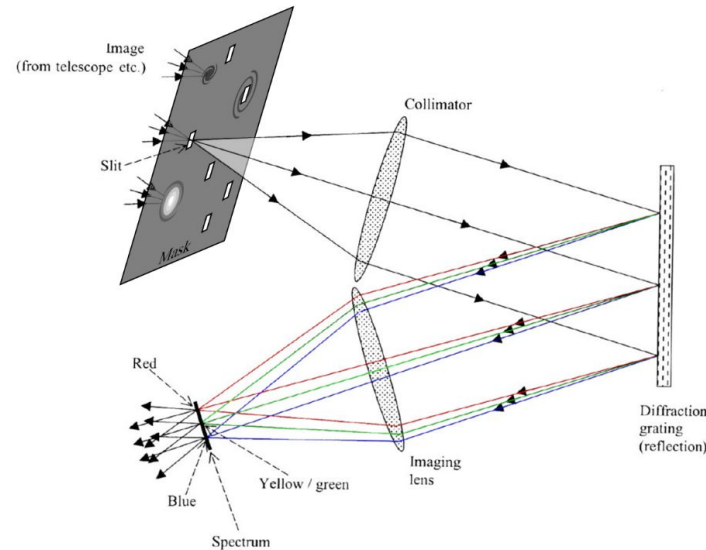
- Spectra \longleftrightarrow Kinematic information
- Absorption and emission features on spectrum
- With templates, we'll know
 - Redshift, Galaxy type, Chemical composition

Spectrographs

1. **Wide field slitless:** for space-based
2. **Long slit:** for nebulae
3. **Multi-object (MOS)**
 - **Mask + Slit** — slit is a key to recover one-dimensional kinematics of galaxy
 - **Fiber + IFU** — any position but fewer targets

Upper — Multi-object spectrograph (MOS).
Lower Left — A mask design.
Lower Right — 2D spectra horizontally diffracted.

Thesis Figure



1. Rotation Curve

Rotational velocity profile (Courteau 1997, Green et al. 2014)

Disk galaxies:

$$V(R) = \frac{2V_a}{\pi} \arctan\left(\frac{R}{R_t}\right)$$

- ❖ As $R \rightarrow \infty$, $V(\infty) = V_a$ (asymptotic velocity).



1. Rotation Curve



Rotational velocity profile (Courteau 1997, Green et al. 2014)

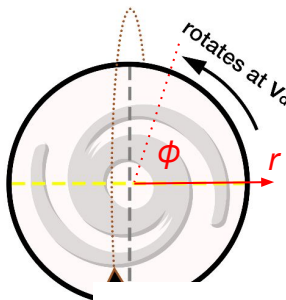
Disk galaxies:

$$V(R) = \frac{2V_a}{\pi} \arctan\left(\frac{R}{R_t}\right)$$

- ❖ As $R \rightarrow \infty$, $V(\infty) = V_a$ (asymptotic velocity).

Velocity Field $\Delta v(r, \phi)$

$$\Delta v(r, \phi) := V(R) = \frac{2V_a}{\pi} \arctan\left(\frac{r(\phi)}{r_t(\phi)}\right)$$



- ❖ r = projected R
- ❖ r_t = projected R_t
- ❖ $V_a = V_a$

1. Rotation Curve



Rotational velocity profile (Courteau 1997, Green et al. 2014)

Disk galaxies:

$$V(R) = \frac{2V_a}{\pi} \arctan\left(\frac{R}{R_t}\right)$$

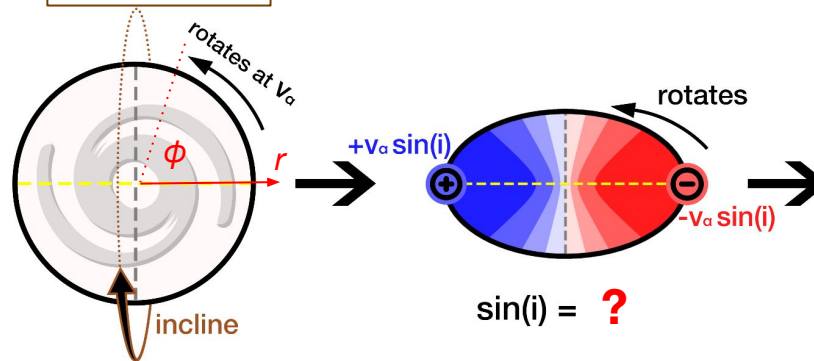
- ❖ As $R \rightarrow \infty$, $V(\infty) = V_a$ (asymptotic velocity).

Velocity Field $\Delta v(r, \phi)$ of an inclined galaxy

$$\Delta v_{\text{los}}(r, \phi) := V(R) \boxed{\cos(\phi) \sin(i)} = \frac{2V_a}{\pi} \boxed{\cos(\phi) \sin(i)} \arctan\left(\frac{r(\phi)}{r_t(\phi)}\right)$$

Light-of-sight component

- ❖ r = projected R
- ❖ r_t = projected R_t
- ❖ $V_a = V_a$



1. Rotation Curve



Rotational velocity profile (Courteau 1997, Green et al. 2014)

Disk galaxies:

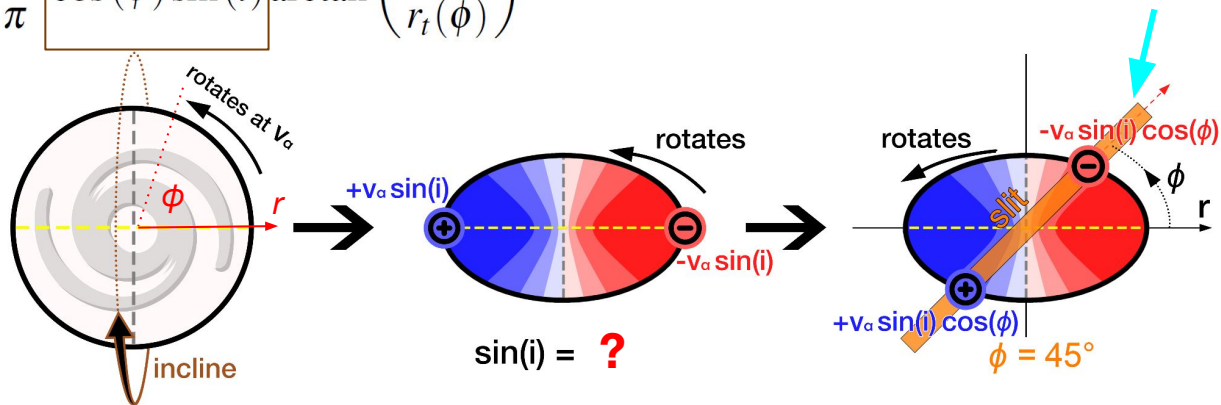
$$V(R) = \frac{2V_a}{\pi} \arctan\left(\frac{R}{R_t}\right)$$

- ❖ As $R \rightarrow \infty$, $V(\infty) = V_a$ (asymptotic velocity).

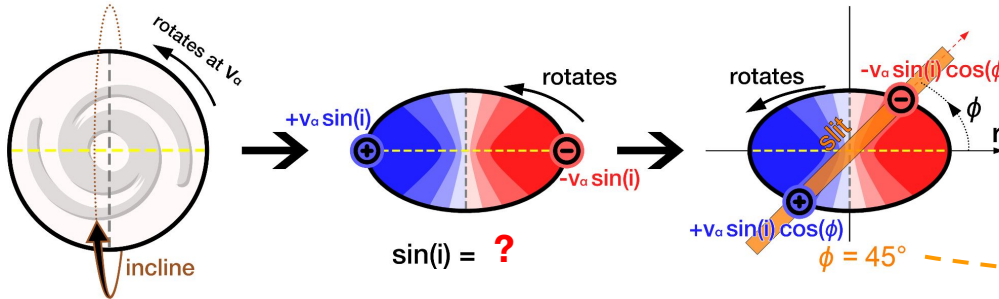
Velocity Field $\Delta v(r, \phi)$ of an inclined galaxy

$$\Delta v_{\text{los}}(r, \phi) := V(R) \boxed{\cos(\phi) \sin(i)} = \frac{2V_a}{\pi} \boxed{\cos(\phi) \sin(i)} \arctan\left(\frac{r(\phi)}{r_t(\phi)}\right)$$

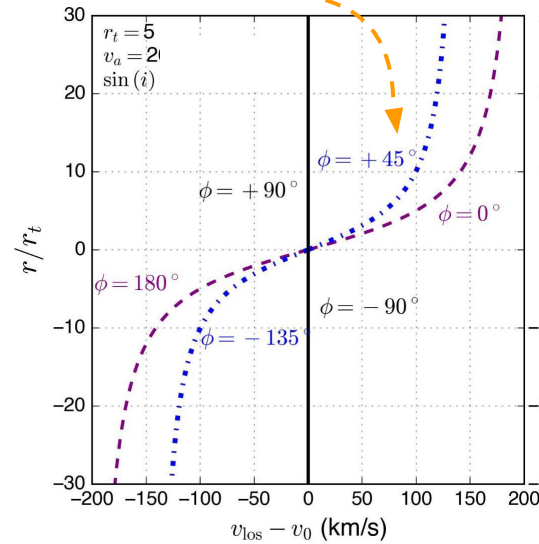
- ❖ r = projected R
- ❖ r_t = projected R_t
- ❖ $V_a = V_a$



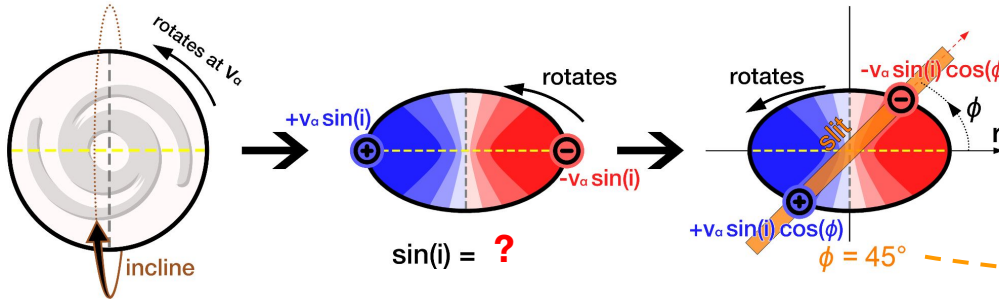
1. Rotation Curve



$$\Delta v_{\text{los}}(r, \phi) := V(R) \cos(\phi) \sin(i) = \frac{2V_a}{\pi} \cos(\phi) \sin(i) \arctan\left(\frac{r(\phi)}{r_t(\phi)}\right)$$

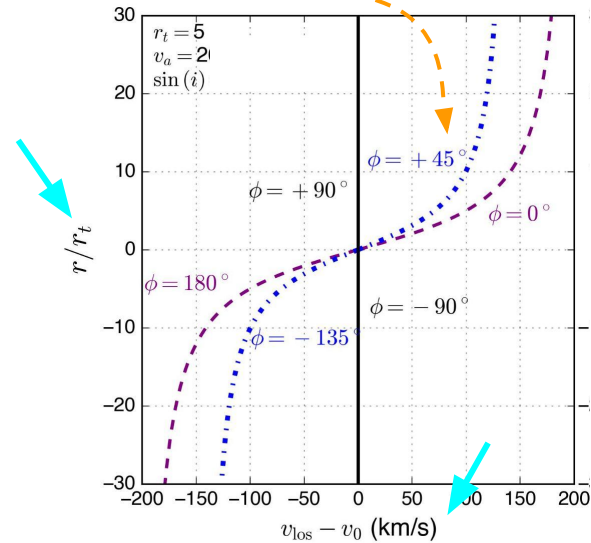


1. Rotation Curve

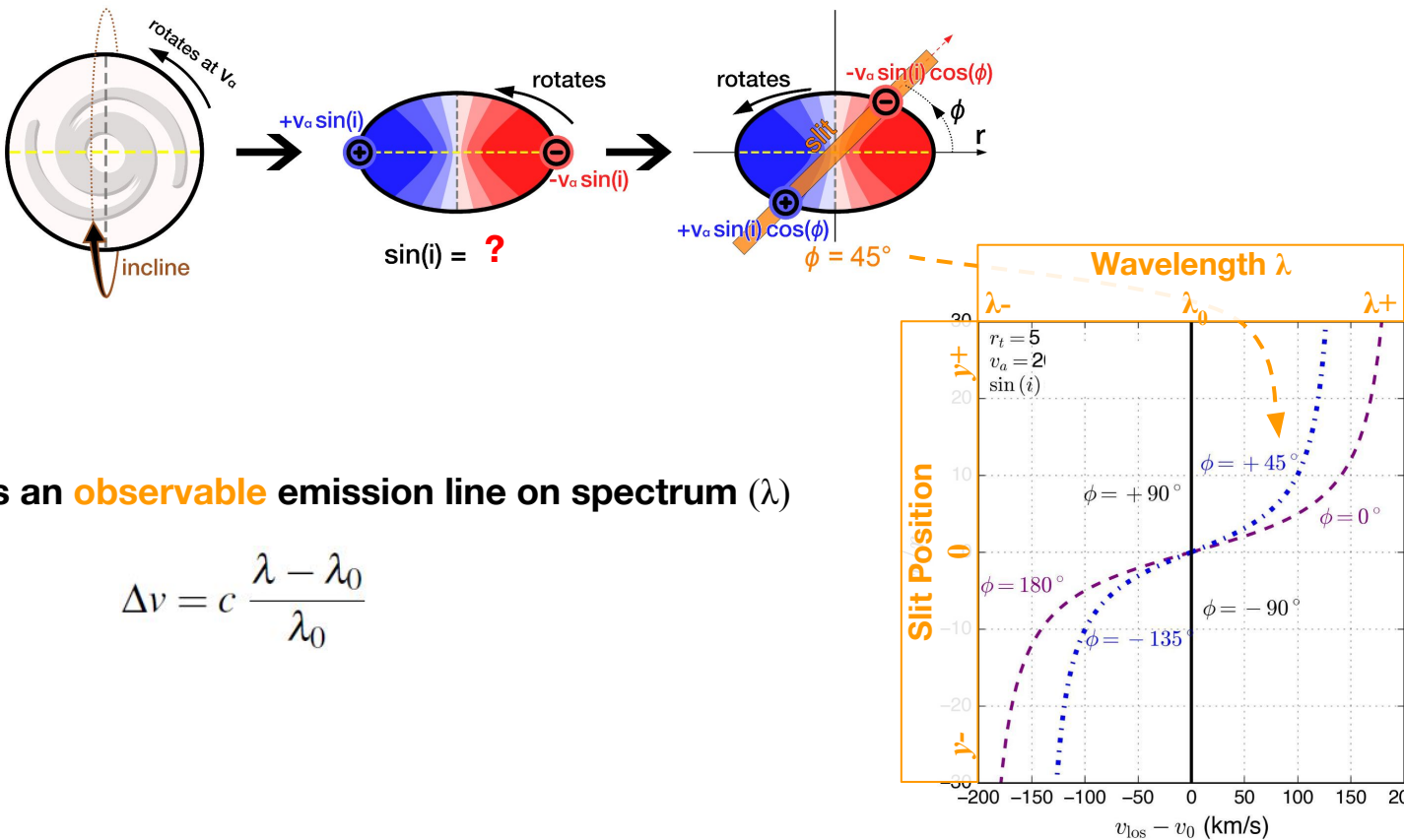


$$\Delta v_{\text{los}}(r, \phi) := V(R) \cos(\phi) \sin(i) = \frac{2V_a}{\pi} \cos(\phi) \sin(i) \arctan\left(\frac{r(\phi)}{r_t(\phi)}\right)$$

$\Delta v(r, \phi)$ with known $\phi \rightarrow \text{Rotation Curve}$

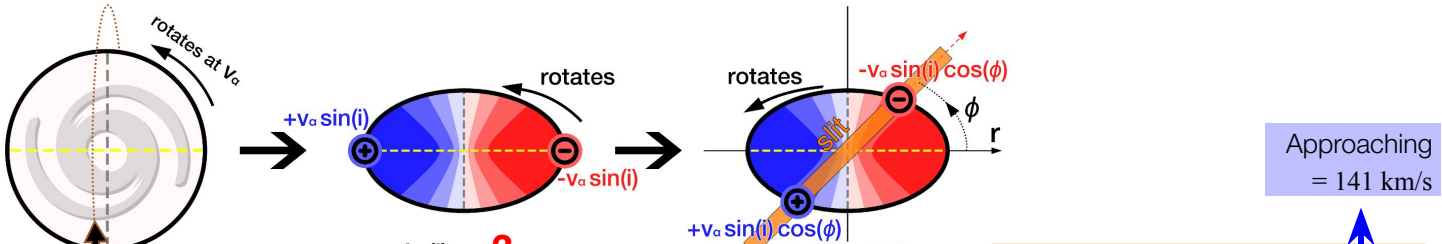


1. Rotation Curve



Rotation Curve is an **observable** emission line on spectrum (λ)

1. Rotation Curve

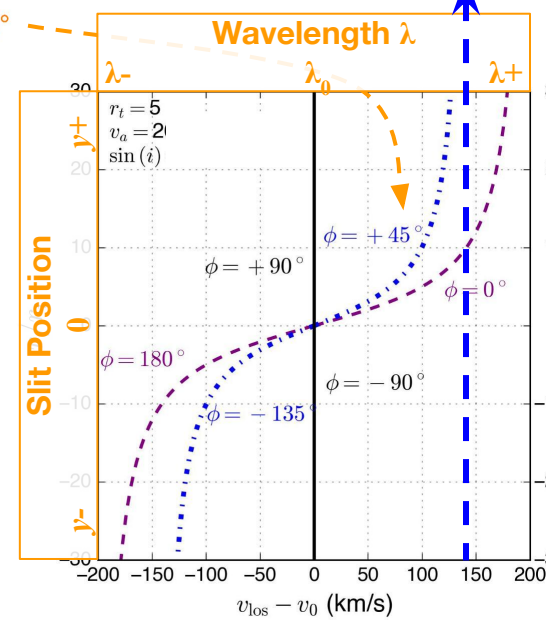


Find asymptotic light-of-sight velocity

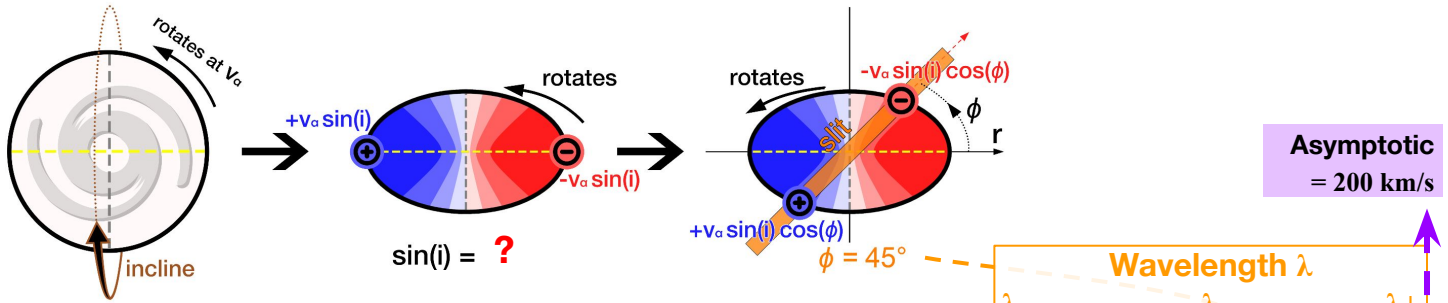
$$\lim_{r \rightarrow \infty} \left[\frac{2V_a}{\pi} \cos(\phi) \sin(i) \arctan \left(\frac{r(\phi)}{r_t(\phi)} \right) \right]$$



$$v_a \cos(\phi) \sin(i)$$



1. Rotation Curve



Find asymptotic light-of-sight velocity *along major axis*

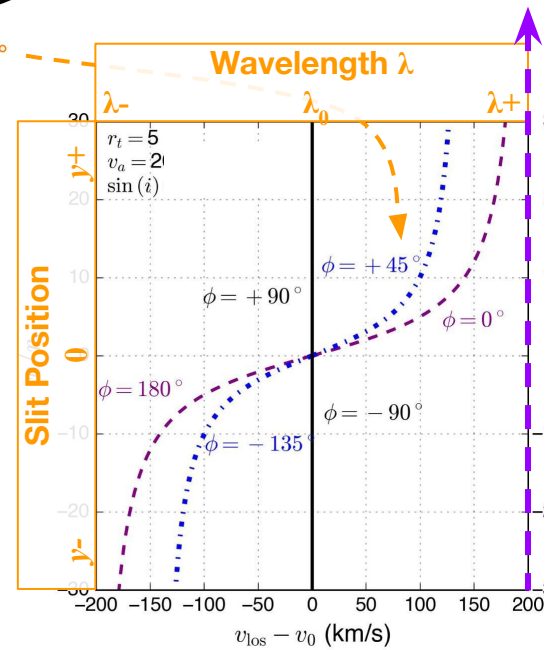
$$\lim_{\substack{r \rightarrow \infty \\ \phi \rightarrow 0}} \left[\frac{2V_a}{\pi} \cos(\phi) \sin(i) \arctan \left(\frac{r(\phi)}{r_t(\phi)} \right) \right]$$

known \square known

$$\lim_{\phi \rightarrow 0} \left[v_a \cos(\phi) \sin(i) \right]$$

known

$$\Delta v_{\max} = \boxed{v_a} \sin(i)$$



2. Maximum Rotational Speed $v_{\text{rot,TF}}$

Tully-Fisher scaling relation (Tully & Fisher 1977)

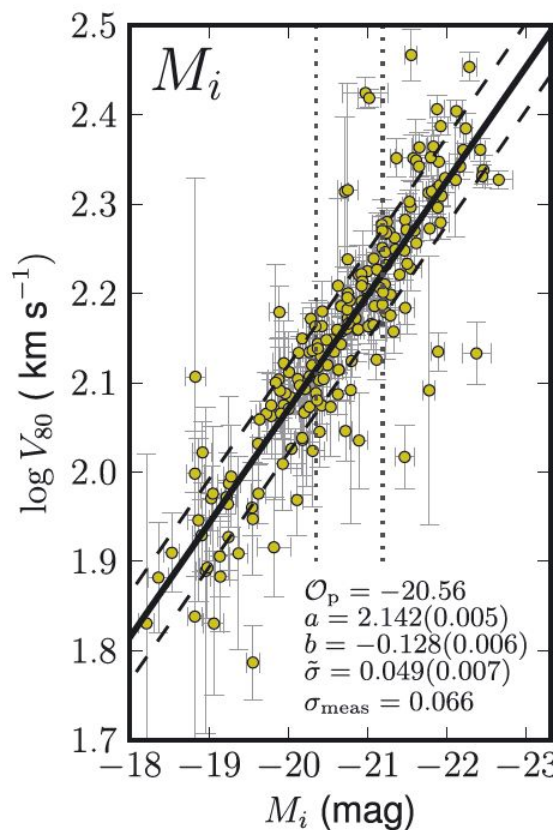
Disk galaxies:

$$\log(v_{\text{rot,TF}}) = a(M_B - M_0) + b$$

↑
Absolute magnitude

SDSS *r*-band galaxies: (Reyes et al. 2011)

$$\log \left(\frac{v_{\text{rot,TF}}}{139^{+1}_{-2} \text{ km s}^{-1}} \right) = \left(-0.130^{+0.007}_{-0.007} \frac{\log(\text{km s}^{-1})}{\text{mag}} \right) (M_r + 20.375 \text{ mag})$$



ITFRs between rotation velocities V_{80} and photometric M_i for the 189 galaxies.

Reyes et al. (2011) Figure 20

Takeaways:

**Maximum Rotational Speed of
Tully-Fisher Relation**

$$\log(v_{\text{rot,TF}}) = a(M_B - M_0) + b$$

**Asymptotic Velocity of
Rotation Curve**

$$\Delta v_{\text{max}} = v_a \sin(i) = \lim_{r \rightarrow \infty} [\Delta v(r, 0)]$$

$$v_a = v_{\text{rot,TF}}$$



Takeaways:

Maximum Rotational Speed of
Tully-Fisher Relation

Asymptotic Velocity of
Rotation Curve

$$\log(v_{\text{rot,TF}}) = a(M_B - M_0) + b$$

$$\Delta v_{\text{max}} = v_a \sin(i) = \lim_{r \rightarrow \infty} [\Delta v(r, 0)]$$

$$v_a = v_{\text{rot,TF}}$$

Galaxy inclination
(intrinsic shape)

$$\sin(i) = \frac{\Delta v_{\text{max}}}{v_{\text{rot,TF}}}$$

Expectations of Kinematic Lensing

KL improves 3 important aspects of
traditional weak lensing systematics from $\sigma_e \sim 0.26$ (LSST)

1. Reduced Shape Noise.

- *Infer the velocity/frequency field of the source galaxy.*
- *Direct outcomes by using those spectrographs with IFUs.*

Expectations of Kinematic Lensing

KL improves 3 important aspects of
traditional weak lensing systematics from $\sigma_e \sim 0.26$ (LSST)

1. Reduced Shape Noise.

- Infer the velocity/frequency field of the source galaxy.
- Direct outcomes by using those spectrographs with IFUs.

2. Redshift Uncertainties.

- Spectroscopic redshifts' better precision, with error of $\Delta_{\text{spec-z}} \sim 0.001$.
- Photometric redshifts ($\Delta_{\text{photo-z}} \sim 0.05$, Tanaka et al. 2018).

Expectations of Kinematic Lensing

KL improves 3 important aspects of
traditional weak lensing systematics from $\sigma_\epsilon \sim 0.26$ (LSST)

1. Reduced Shape Noise.

- Infer the velocity/frequency field of the source galaxy.
- Direct outcomes by using those spectrographs with IFUs.

2. Redshift Uncertainties.

- Spectroscopic redshifts' better precision, with error of $\Delta_{\text{spec-z}} \sim 0.001$.
- Photometric redshifts ($\Delta_{\text{photo-z}} \sim 0.05$, Tanaka et al. 2018).

3. More Bright Galaxy Samples.

- Traditional lensing: **must include low SNR galaxies** (e.g., J+H band combined SNR>18, Eifler et al. 2021) to increase the sample size and statistical precision.
- However, **KL: r-band SNR>50**, emission-line-well-resolved, unblended (relatively isolated) galaxies, improving the photometric shape measurement for smaller biases (Pranjal et al. 2023, Xu et al. 2023).

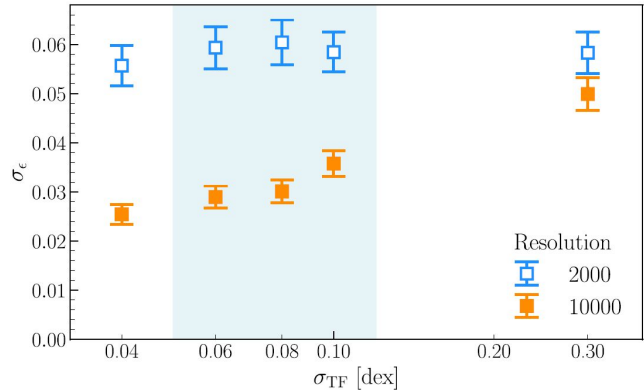
KL Shape Noise: $\sigma_\epsilon^{\text{KL}} = 0.04$ from the recent mock observations (Pranjal et al. 2023)

Expectations of Kinematic Lensing

KL shape noise $\sigma_{\epsilon}^{\text{KL}} = 0.04$ depends on the following systematics:

1. Tully-Fisher Relation Intrinsic Scatter (σ_{TF})

- $R = 2000$ resolving power + spectral SNR=30,
an average of $\sigma_{\epsilon}^{\text{KL}} = 0.06$ (Pranjali et al. 2023)

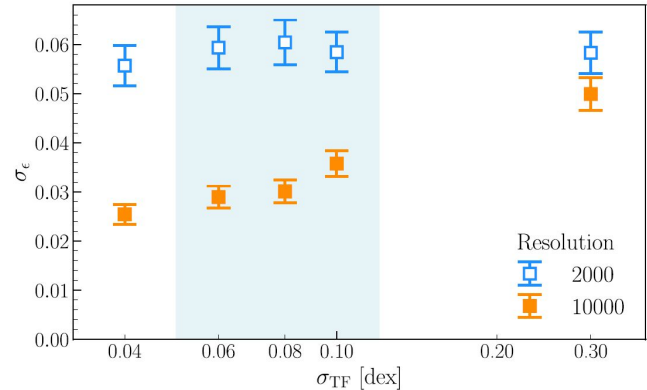


Expectations of Kinematic Lensing

KL shape noise $\sigma_{\epsilon}^{\text{KL}} = 0.04$ depends on the following systematics:

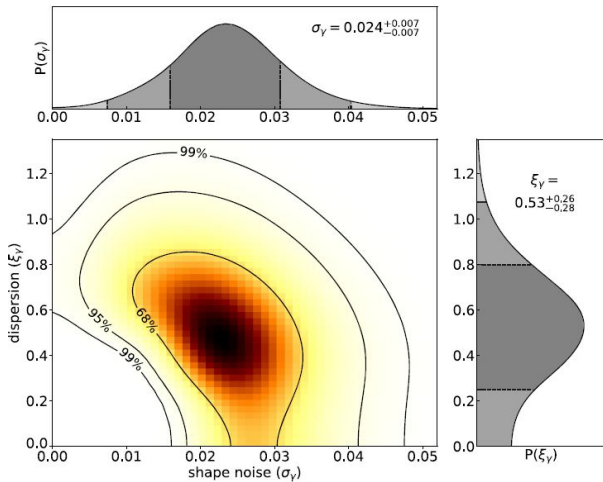
1. Tully-Fisher Relation Intrinsic Scatter (σ_{TF})

- $R = 2000$ resolving power + spectral SNR=30,
an average of $\sigma_{\epsilon}^{\text{KL}} = 0.06$ (Pranjal et al. 2023)



Importance of the velocity fields inferred by spectroscopy

- Gurri et al. (2020) — galaxy-galaxy lensing systems;
use the lens-source position relation to infer v_a
- Gurri et al. (2021) and DiGiorgio et al. (2021) — effective shape noise $\sigma_{\epsilon} = 0.017\text{--}0.031$
- Wittman & Self (2021) — involve Tully-Fisher relation; shape noise of $\sigma_{\epsilon} \sim 0.04$



Kinematic Lensing on “Weighing the Giants” Galaxy Clusters with Keck/DEIMOS

Mining in the archived slit-spectroscopic data

Target Selection

“Weighing the Giants” project galaxy cluster sample

(51 clusters; von der Linden et al. 2014a,b, Kelly et al. 2014, and Applegate et al. 2014)

“Weighing the Giants” (*WtG*) clusters

- calibrated with robust weak-lensing masses from X-ray observations
- span an intermediate redshift range of $0.15 < z_{\text{cl}} < 0.7$.
 - (1) Photometric imaging observed with Subaru/SuprimeCam and CFHT/MegaPrime;
 - (2) Maps of the total mass distribution measured from weak lensing;
 - (3) **Robust weak-lensing shape measurement at hand;**
 - (4) Central galaxy determination; and
 - (5) Photometric redshifts.

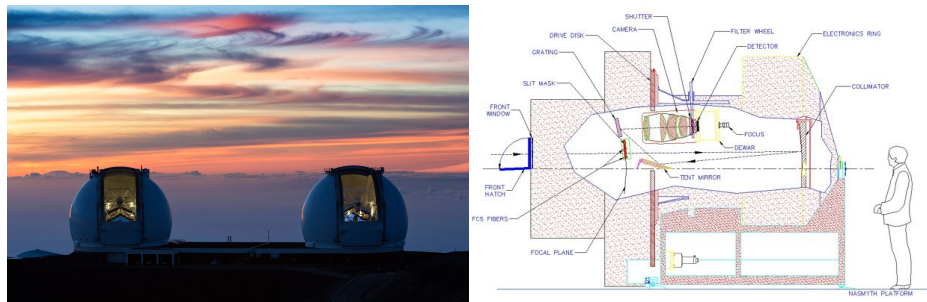
Target Selection

“Weighing the Giants” project galaxy cluster sample
(51 clusters; von der Linden et al. 2014a,b, Kelly et al. 2014, and Applegate et al. 2014)

Keck/DEIMOS instrument
(Faber et al. 2003)

Keck/DEIMOS (DEep Imaging Multi-Object Spectrograph; Faber et al. 2003)

- Visible-wavelength, faint-object, multi-slit imaging spectrograph of Keck II telescope
- Wavelength range of 4100–11000 Å
 - Ca H&K $\lambda\lambda$ 3933,3968 doublet (absorption)
 - [O II] $\lambda\lambda$ 3727,3729 doublet
 - [S II] $\lambda\lambda$ 6716,6731 doublet,
[O III] $\lambda\lambda$ 4959,5007 doublet,
N II $\lambda\lambda$ 6548,6584 doublet, &
H γ λ 4340, H β λ 4861, H α λ 6563.



Spectroscopic Grating (lines/mm)	Blaze Wavelength (Å)	Dispersion Scale (Å/pixel)	FWHM Spectral Resolution (1'' slit) $\Delta\lambda$ (Å)	Resolving Power R
600	7500	0.65	4.7	1606
1200	7500	0.33	1.5–2.1	3571–5000

This thesis
(6 clusters + 17 masks)

“Weighing the Giants” project galaxy cluster sample
(51 clusters; von der Linden et al. 2014a,b, Kelly et al. 2014, and Applegate et al. 2014)

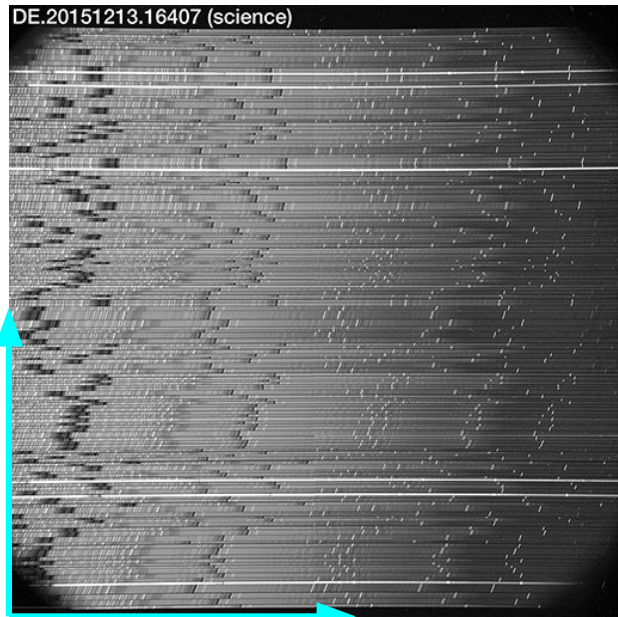
Keck/DEIMOS instrument
(Faber et al. 2003)

	Cluster	RA (deg)	Dec. (deg)	z_{Cl}	M10	Mask	Grating	Date	Set
	(1)	(2)	(3)	(4)	(5)	(6)	(7)	(8)	(9)
1	A2552	347.88818	3.63514	0.302	M	25521B	1200G	2015-12-13	A
2	A611	120.23674	36.05709	0.288	–	sna611	600ZD	2012-10-15	E
3	A1758N	203.18111	50.54398	0.279	–	ejc	600ZD	2018-07-16	I
4	A1758N	203.18111	50.54398	0.279	–	ejc1	600ZD	2018-07-17	C
5	A1758N	203.18111	50.54398	0.279	–	ejc2	600ZD	2018-07-18	D
6	M1115	168.96617	1.49861	0.355	M	sn1115	600ZD	2012-02-26	B
7	M1115	168.96617	1.49861	0.355	M	1115m1	600ZD	2014-02-25	A
8	M1115	168.96617	1.49861	0.355	M	jc9	600ZD	2015-06-16	B
9	A2261	260.61244	32.13275	0.224	B	a2261aB	1200G	2014-07-01	A
10	A2261	260.61244	32.13275	0.224	B	a2261b	1200G	2014-07-01	B
11	A2261	260.61244	32.13275	0.224	B	a2261c	1200G	2014-07-01	C
12	A2261	260.61244	32.13275	0.224	B	a2261d	1200G	2015-06-18	A
13	A2261	260.61244	32.13275	0.224	B	a2261c	1200G	2015-06-18	B
14	A2261	260.61244	32.13275	0.224	B	a2261b	1200G	2015-06-18	C
15	A2261	260.61244	32.13275	0.224	B	a2261a	1200G	2015-06-18	D
16	A370	39.97186	-1.57718	0.375	–	A37017B1	1200G	2017-09-28	A
17	A370	39.97186	-1.57718	0.375	–	A37017B2	1200G	2017-09-28	B

Data Reduction

Raw and Calibration Data

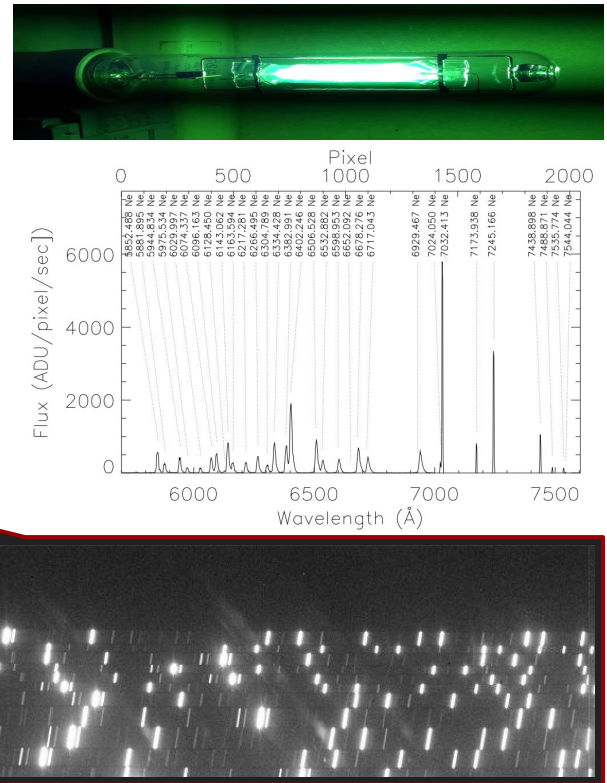
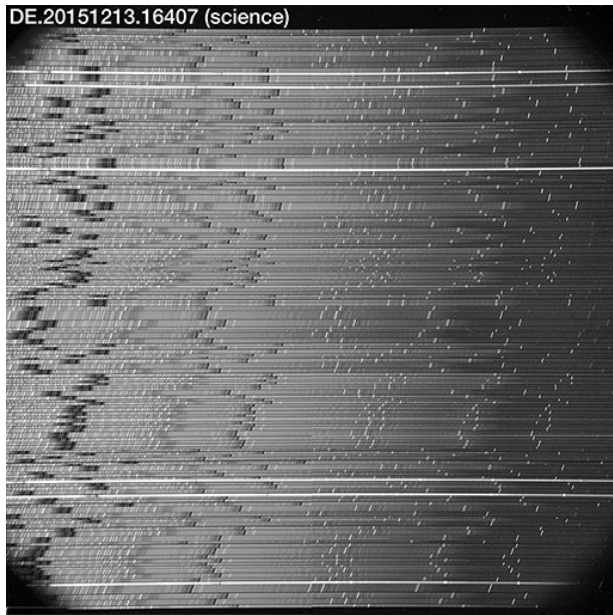
CCD 8192×8192 pixel² science image of
the cluster A2552's spectra



Data Reduction

Raw and Calibration Data

“Arc image” maps the pixel position to wavelengths → Identify wavelength at each x-pixel (Right plots: ${}_{10}\text{Ne}$ arc lamp flux-wavelength plot from Keck/Iris)

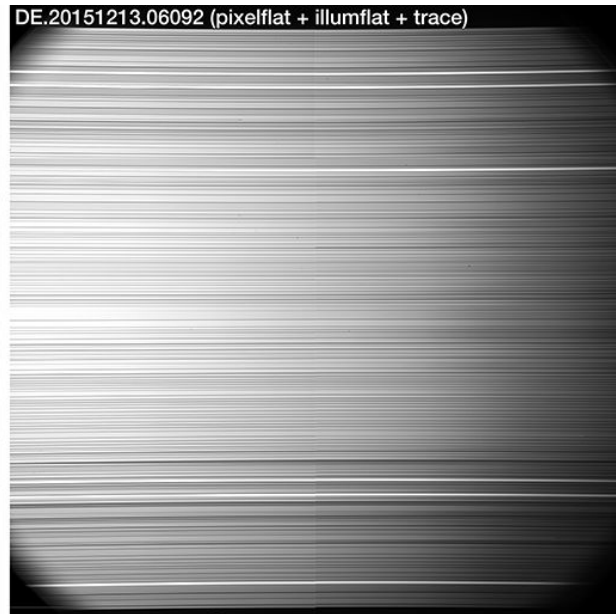
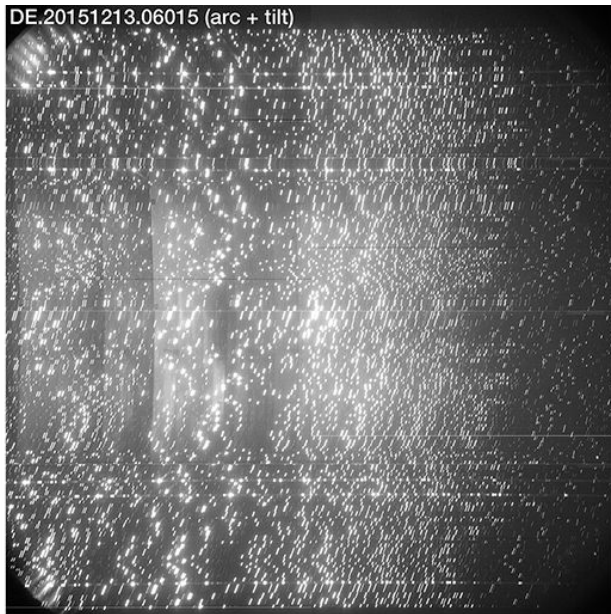
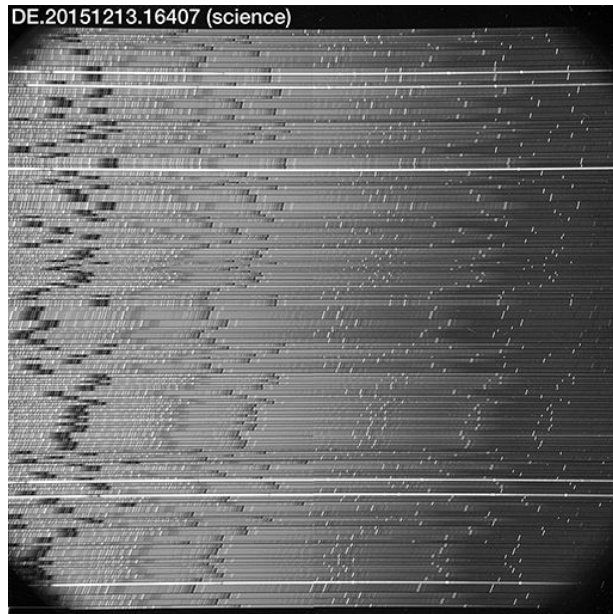


Data Reduction

Raw and Calibration Data

“Trace image” also traces the dispersion directions of slits.

They are edges of slits.



Data Reduction — PypeIt

Python-based pipeline for the popular MOS instruments



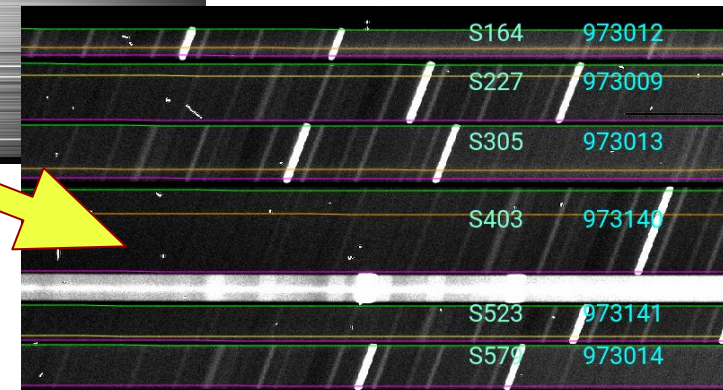
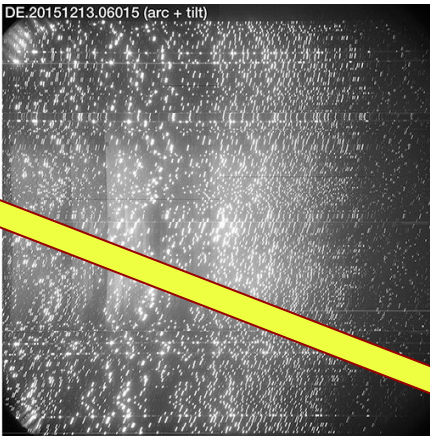
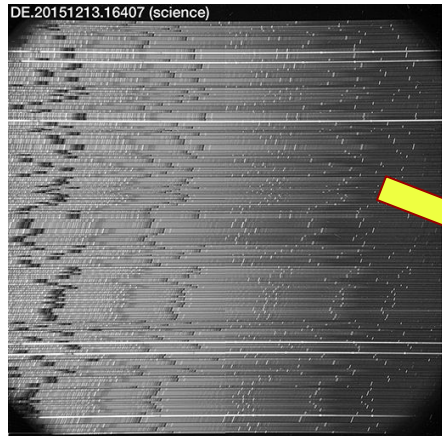
Data Reduction — PypeIt

Python-based pipeline for the popular MOS instruments



Slit Identification

Which slit \longleftrightarrow which 2D spectrum strip



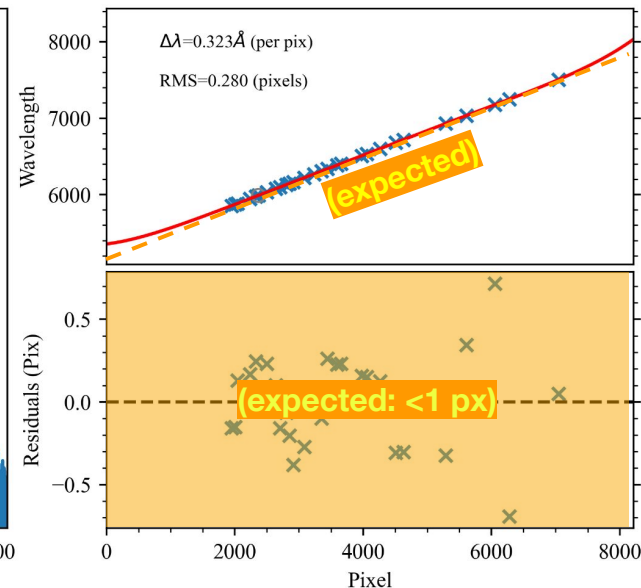
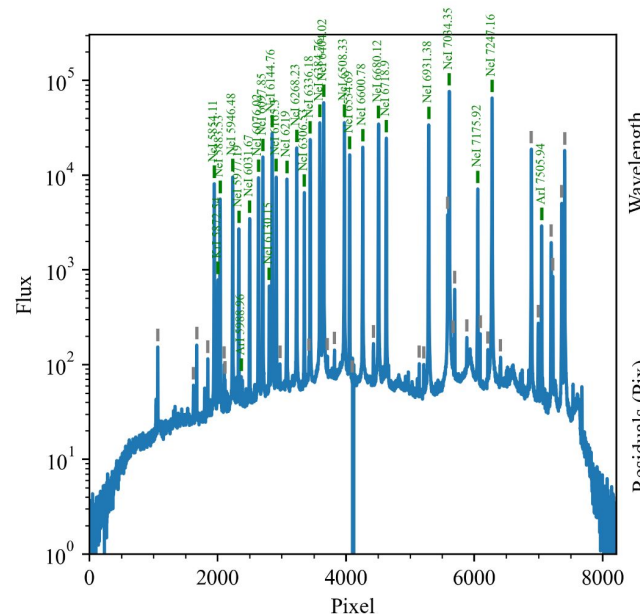
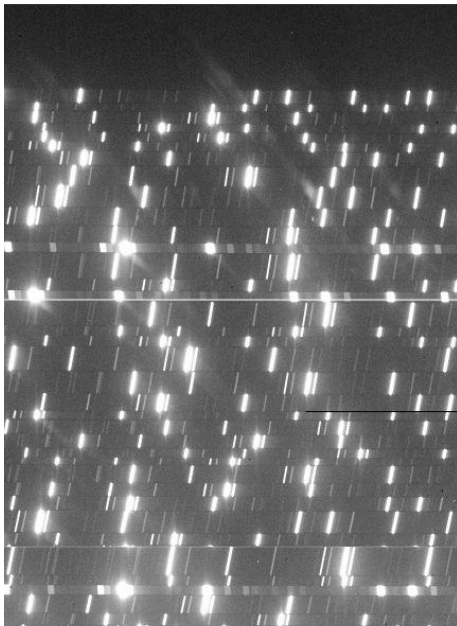
Data Reduction — PypeIt *Python-based pipeline for the popular MOS instruments*



Wavelength Calibration

PypeIt identifies arc lines.

TypeIT determines pixel-wavelength mapping and gives analytic polynomial fit.



Data Reduction — PypeIt

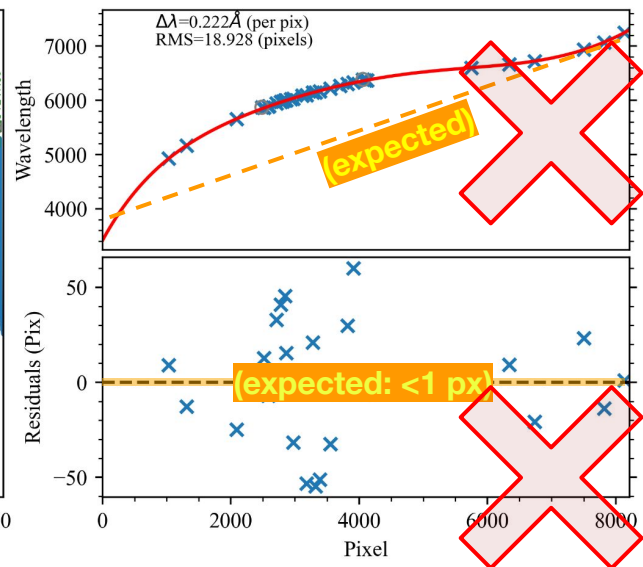
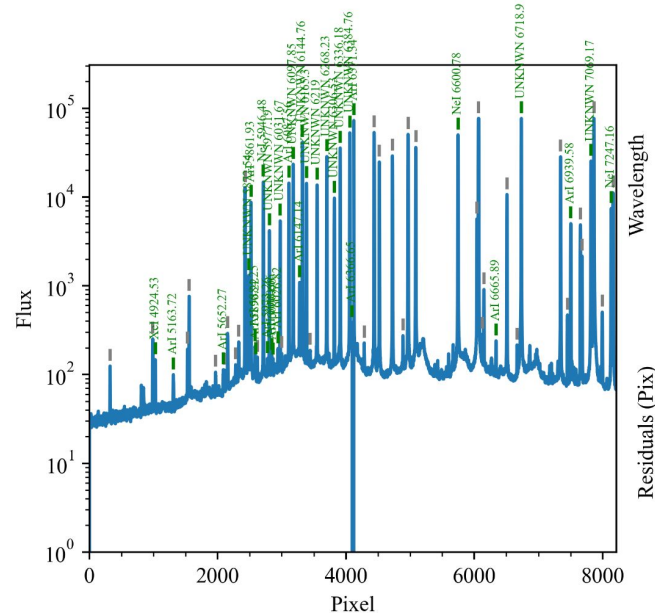
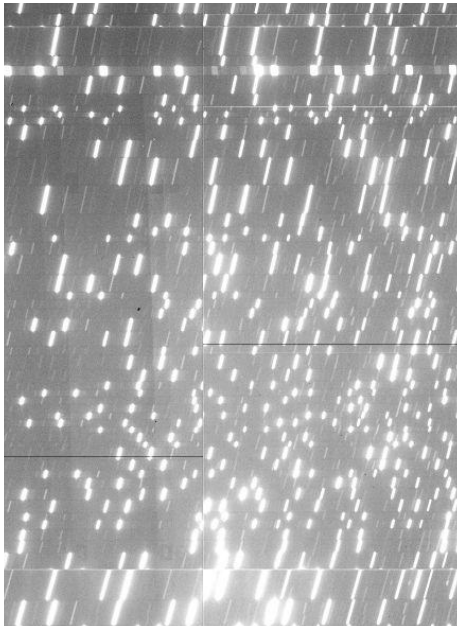
PypeIt: Python-based pipeline for the popular MOS instruments



Wavelength Calibration

PypeIt identifies arc lines.

PypeIt determines pixel-wavelength mapping and gives analytic polynomial fit.



Data Reduction — PypeIt

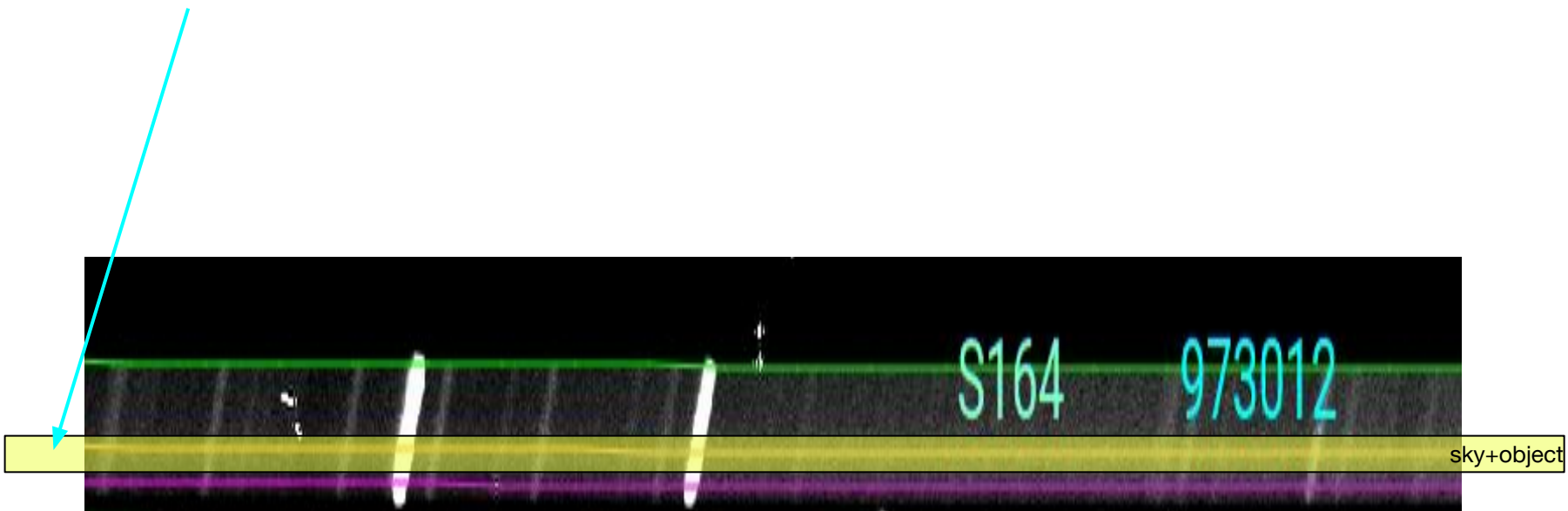
Python-based pipeline for the popular MOS instruments



Object Finding and Sky Line Subtraction

Sky lines are a series of lines illuminated by atmospheric airflow

- **2D object model** (continuum-like) — Pixels with **higher SNRs** (e.g., $\text{SNR} > 5\sigma$)



Data Reduction — PypeIt

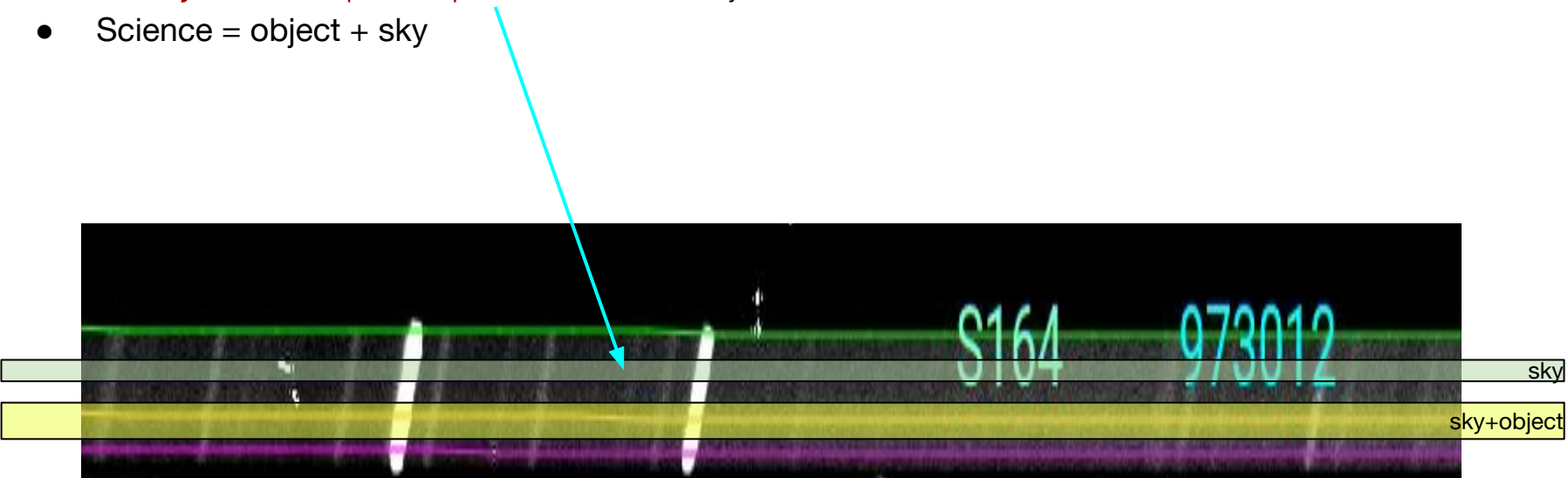
Python-based pipeline for the popular MOS instruments



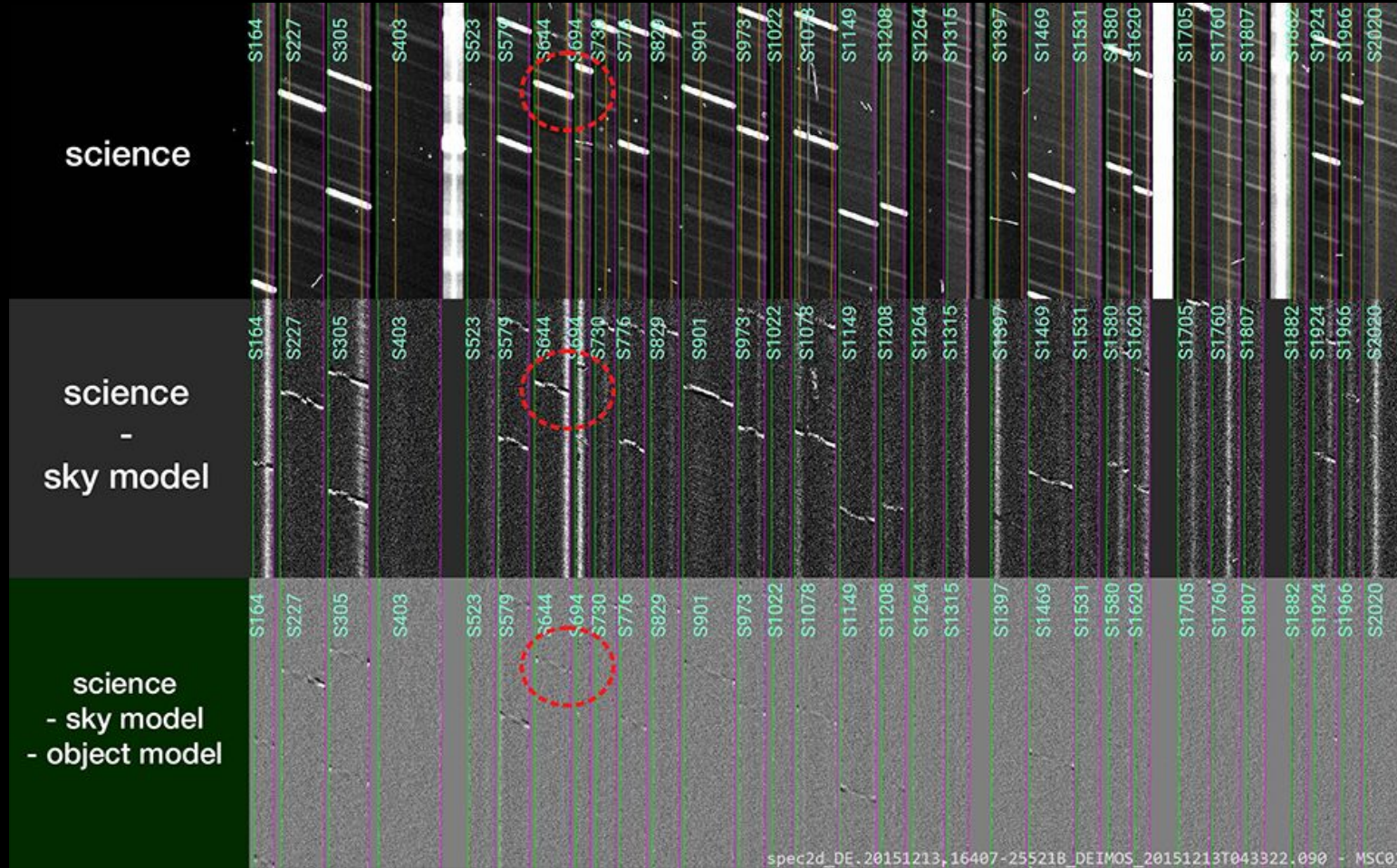
Object Finding and Sky Line Subtraction

Sky lines are a series of lines illuminated by atmospheric airflow

- 2D object model (continuum-like) — Pixels with higher SNRs (e.g., $\text{SNR} > 5\sigma$)
- 2D sky model — parallel pixels next to 2D object
- Science = object + sky



Sky Line Subtraction



Data Reduction — PypeIt

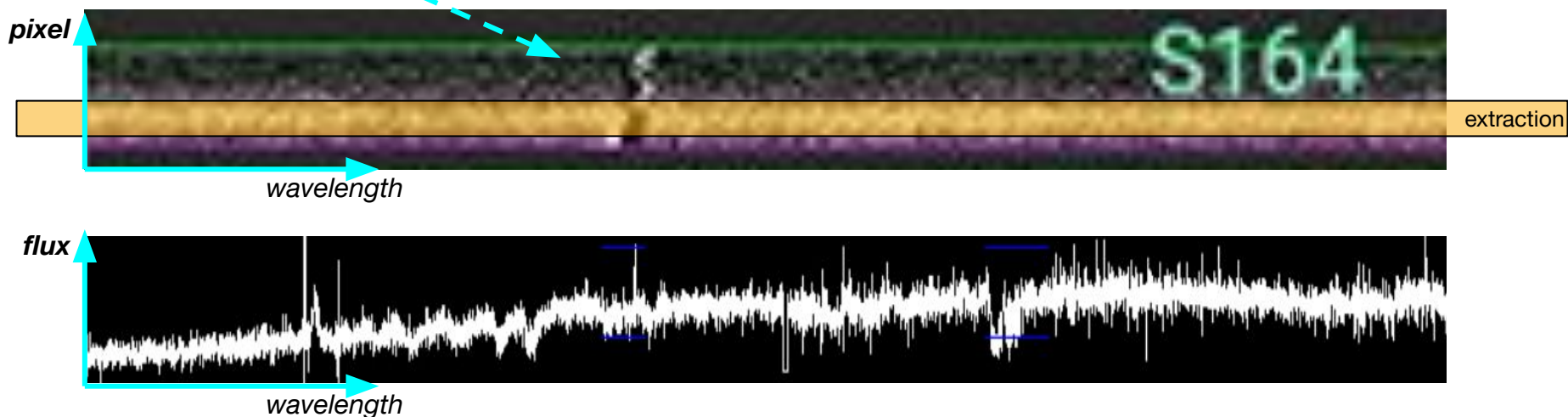
Python-based pipeline for the popular MOS instruments



1D spectrum

Define an extraction width.

The flux of **2D object** is integrated into 1D spectrum model.



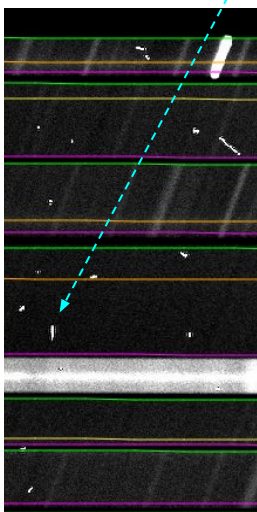
Data Reduction — PypeIt



Co-addition

Remove cosmic rays

Co-add multiple frames to the weighted mean (an average image using uniform weighting).



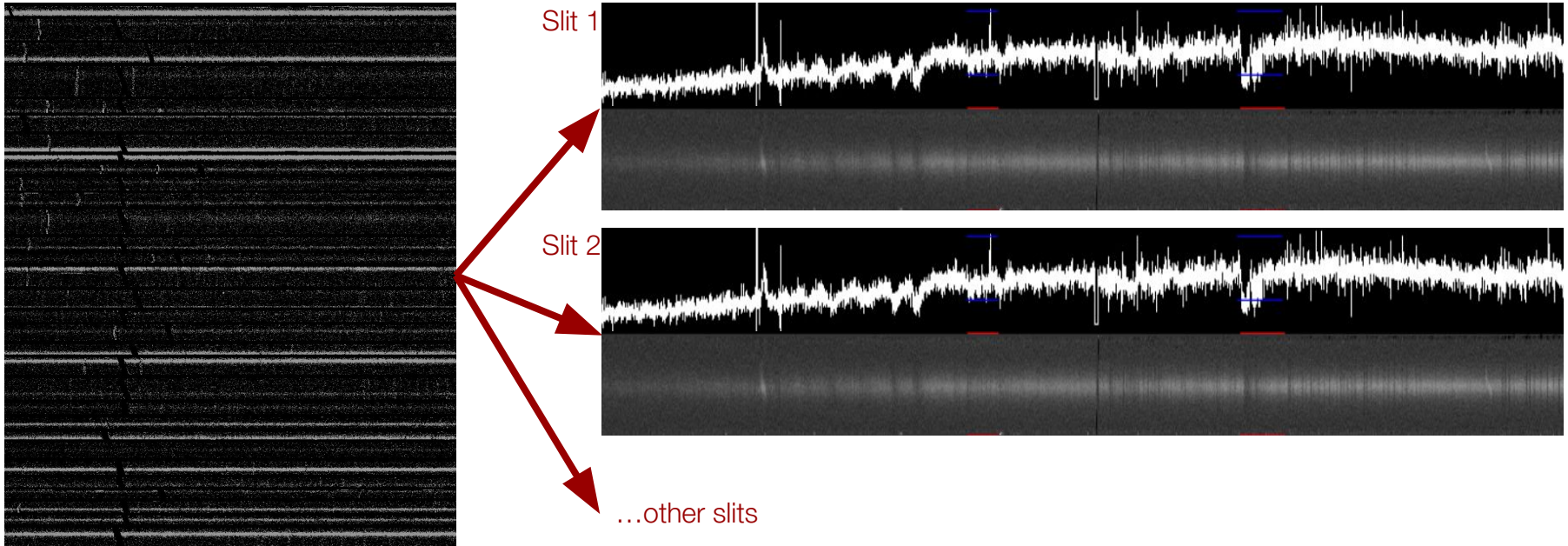
Results

Spectroscopic Redshift

Results

Spectroscopic Redshift

1. Spectrum Cutting-off by Slit — `pypeittospecpro.py` | 1338 spectra | 1125 targets



Results

Spectroscopic Redshift

1. Spectrum Cutting-off by Slit
2. Templates

Table 2.3: Spectral Templates For Cross-Correlation

Template	Source	Dispersion Scale (Å/pixel)	Spectral Resolution $\Delta\lambda$ (Å)	Resolving Power R
LBG Shapley	Lyman break galaxy○	1.0	8–12	417–625
SDSS QSO	Broad-line quasar△	1.0	2	2000
SDSS LoBAL	Low-ionization BAL quasar†	0.7	1.8–5.1	2000
SDSS HiBAL	High-ionization BAL quasar†	0.7	1.8–5.1	2000
SDSS Luminous Red	Luminous red galaxy*	1.6	1.8–5.1	2000
SDSS Early Type	Early-type galaxy*	2.1	1.8–5.1	2000
SDSS Low Emission	Low-emission-peak galaxy*	2.1	1.8–5.1	2000
SDSS Normal Emission	Normal-emission-peak galaxy*	2.1	1.8–5.1	2000
SDSS High Emission	High-emission-peak galaxy*	2.1	1.8–5.1	2000
SDSS Late Type	Late-type galaxy*	2.1	1.8–5.1	2000
Red galaxy	PEGASE passive galaxy	2.0	1.4	
Green galaxy	PEGASE early spiral	2.0	1.4	
Blue galaxy	PEGASE spiral/starburst	2.0	1.4	
A0 star	A0 stellar templates‡	5	5	500
F0 star	F0 stellar templates‡	5	5	500
G0 star	G0 stellar templates‡	5	5	500
K0 star	K0 stellar templates‡	5	5	500
M0 star	M0 stellar templates‡	5	5	500
M6 star	M6 stellar templates‡	5	5	500

NOTE — Sources: ○ Shapley et al. (2003), △ Schneider et al. (2010), † Reichard et al. (2003),

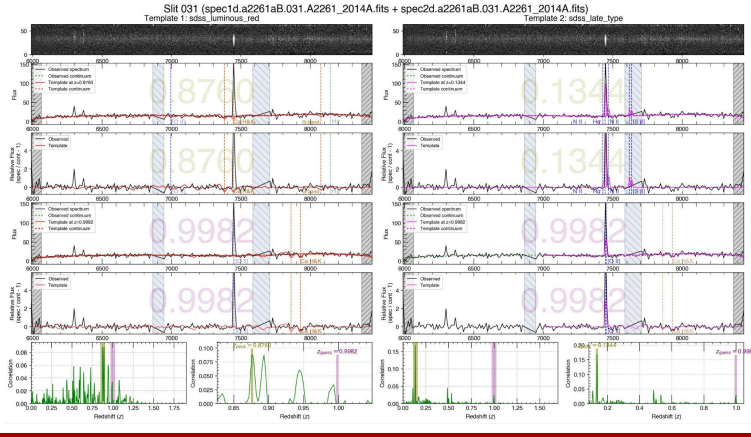
‡ Pickles (1998), and *SDSS DR2 (Abazajian et al. 2004) spectral templates:

<https://classic.sdss.org/dr5/algorithms/spectemplates/index.php>

Results

Spectroscopic Redshift

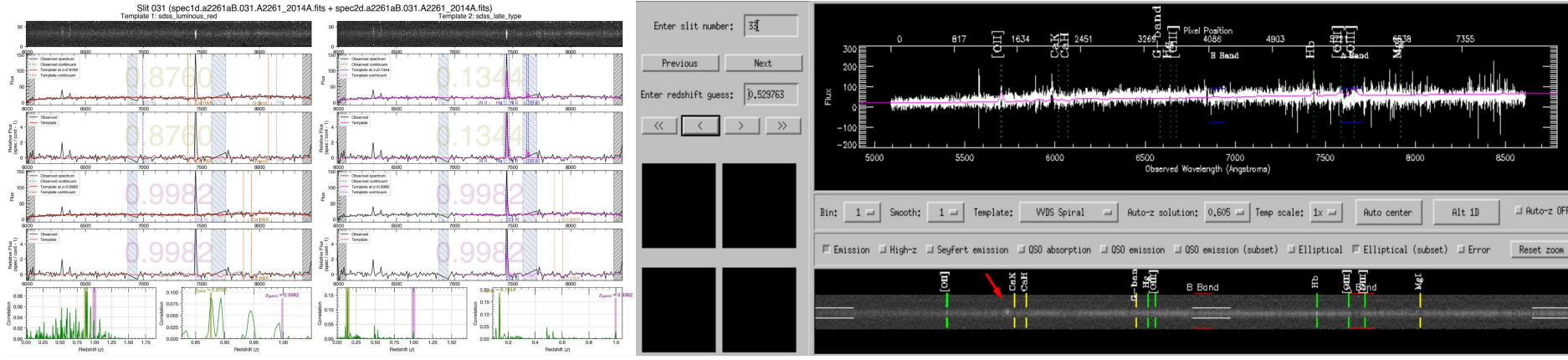
1. Spectrum Cutting-off by Slit — `pypeittospecpro.py` | 1338 spectra | 1125 targets
2. Templates
3. Tools
 - o **FIREFLY** (Fast Initial REdshift Fitting of cLuster galaxY) — for rapid fittings to guess the approximate redshift solutions with probability distribution.



Results

Spectroscopic Redshift

1. Spectrum Cutting-off by Slit — pypeittospecpro.py | 1338 spectra | 1125 targets
2. Templates
3. Tools
 - o **FIREFLY** (Fast Initial REdshift Fitting of cLuster galaxY) — for **rapid fittings** to guess the **approximate redshift** solutions with probability distribution.
 - o **IDL/SpecPro** (Masters & Capak 2011) — user **visual** inspections in GUI + **manual** redshift adjustments to fit with the template best visually.



Results

Spectroscopic Redshift

1. Spectrum Cutting-off by Slit — pypeittospecpro.py | 1338 spectra | 1125 targets
2. Templates
3. Tools — FIREFLY + IDL/SpecPro
4. Secure Redshifts
 - o “confidence” flags — indicate the reliability of spec-z
 - i. **3 = secure** (two or more lines are identified and outcome one redshift)
 - ii. **2 = likely** (one line is identified and outcomes a redshift)
 - iii. 1 = no determination

Results

Spectroscopic Redshift

1. Spectrum Cutting-off by Slit — pypeittospecpro.py | 1338 spectra | 1125 targets
2. Templates
3. Tools — FIREFLY + IDL/SpecPro
4. Secure Redshifts
 - o “confidence” flags — indicate the reliability of spec-z (**3 = secure, 2 = likely, 1 = no determination**)
 - o confidence-flag distribution of 60, 1, and 39% for confidence = 1, 2, and 3

Results

Spectroscopic Redshift

1. Spectrum Cutting-off by Slit — pypeittospecpro.py | 1338 spectra | 1125 targets
2. Templates
3. Tools — FIREFLY + IDL/SpecPro
4. Secure Redshifts
 - o “confidence” flags — indicate the reliability of spec-z (3 = secure, 2 = likely, 1 = no determination)
 - o confidence-flag distribution of 60, 1, and 39% for confidence = 1, 2, and 3
 - o 1125 slit targets produce **451 redshifts of confidence \geq 2**
 - o 8 redshifts with confidence = 3 are for **stars**
 - o **443 redshifts** with the **confidence \geq 2** for non-stellar objects are defined as **secure redshifts**

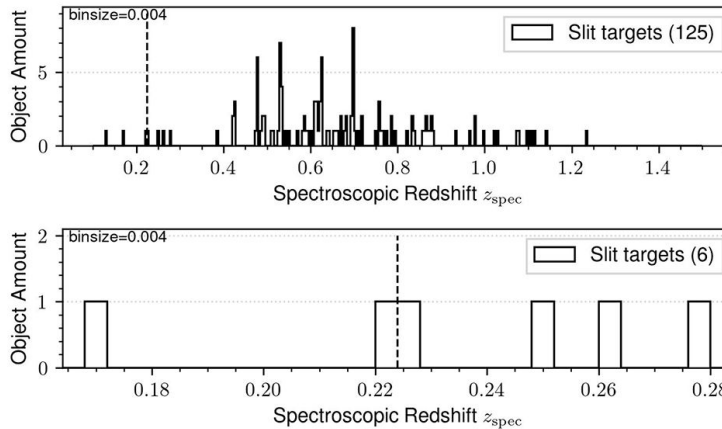
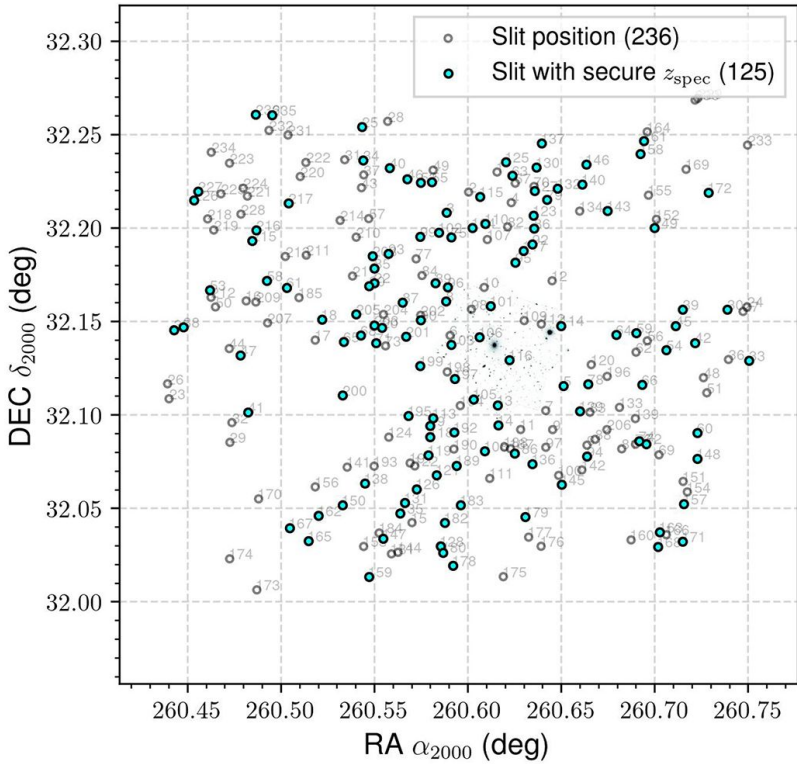
Results

Spectroscopic Redshift

	Cluster	RA (deg)	Dec. (deg)	z_{Cl}	M10	Mask	Grating	Date	Set	N_{slits}	N_z	N_b	N_c	N_{bc}	
	(1)	(2)	(3)	(4)	(5)	(6)	(7)	(8)	(9)	(10)	(11)	(12)	(13)	(14)	
1	A2552	347.88818	3.63514	0.302	M	25521B	1200G	2015-12-13	A	143	72	9	7	2	
2	A611	120.23674	36.05709	0.288	–	sna611	600ZD	2012-10-15	E	48	16	3	2	1	
3	A1758N	203.18111	50.54398	0.279	–	ejc	600ZD	2018-07-16	I	76	22	0	0	0	
4	A1758N	203.18111	50.54398	0.279	–	ejc1	600ZD	2018-07-17	C	63	22	1	0	0	
5	A1758N	203.18111	50.54398	0.279	–	ejc2	600ZD	2018-07-18	D	39	17	2	4	0	
6	M1115	168.96617	1.49861	0.355	M	sn1115	600ZD	2012-02-26	B	120	60	37	15	11	
7	M1115	168.96617	1.49861	0.355	M	1115m1	600ZD	2014-02-25	A	147	76	15	20	3	
8	M1115	168.96617	1.49861	0.355	M	jc9	600ZD	2015-06-16	B	31	11	0	4	0	
9	A2261	260.61244	32.13275	0.224	B	a2261aB	1200G	2014-07-01	A	63	41	37	28	24	
10	A2261	260.61244	32.13275	0.224	B	a2261b	1200G	2014-07-01	B	66	31	31	25	25	
11	A2261	260.61244	32.13275	0.224	B	a2261c	1200G	2014-07-01	C	62	27	26	22	21	
12	A2261	260.61244	32.13275	0.224	B	a2261d	1200G	2015-06-18	A	65	25	25	13	13	
13	A2261	260.61244	32.13275	0.224	B	a2261e	1200G	2015-06-18	B	62	30	29	22	20	
14	A2261	260.61244	32.13275	0.224	B	a2261b	1200G	2015-06-18	C	64	30	28	20	17	
15	A2261	260.61244	32.13275	0.224	B	a2261a	1200G	2015-06-18	D	65	32	29	26	23	
16	A370	39.97186	-1.57718	0.375	–	A37017B1	1200G	2017-09-28	A	121	14	1	4	1	
17	A370	39.97186	-1.57718	0.375	–	A37017B2	1200G	2017-09-28	B	103	11	4	7	1	
										Total	1338	451	277	219	162
										Non-duplicate and Non-Stellar Objects Total	1125	443	187	149	105

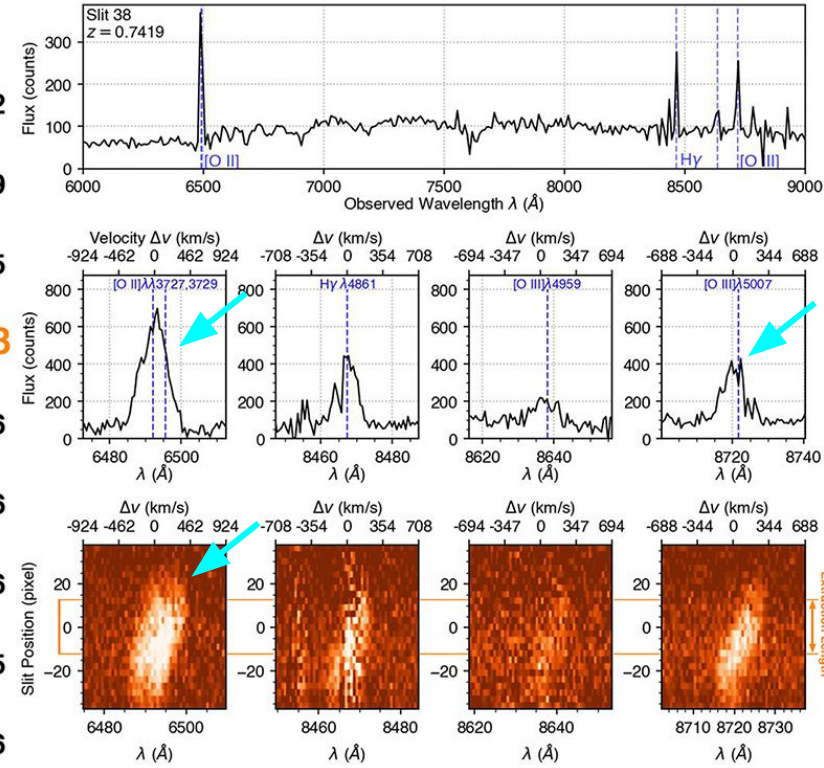
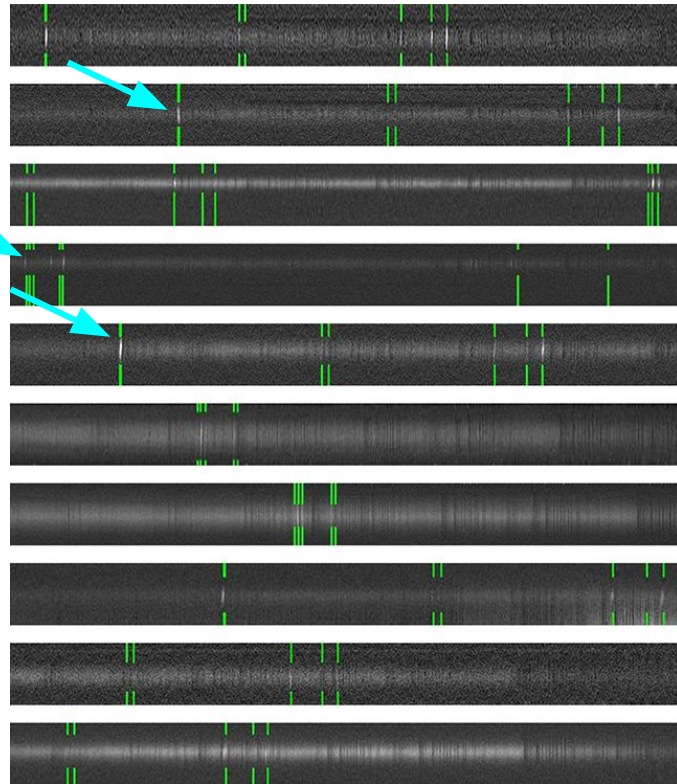
Results

Spectroscopic Redshift



Results

Rotation Curves and Velocity Fields

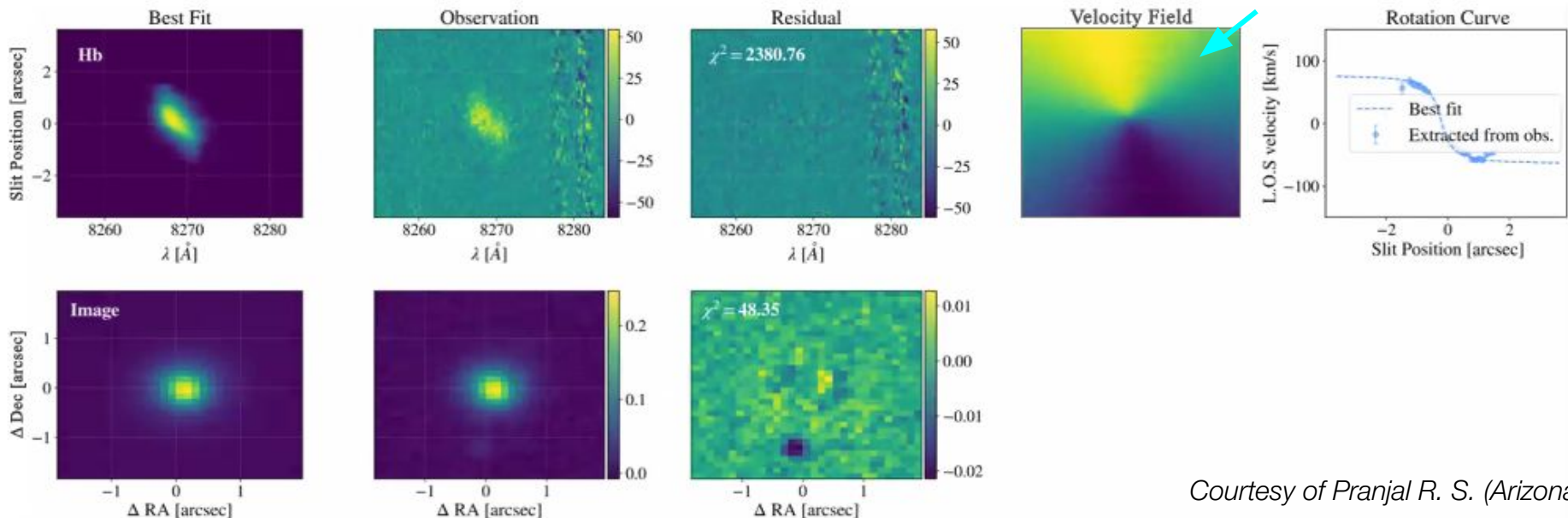


Results

Rotation Curves and Velocity Fields

KL measurement pipeline developed by Pranjal et al. (2023) and fit with the fast-forward model of 20 free parameters:

- γ_t — perpendicular shear component relative to the cluster center
- v_{circ} — Maximum rotational speed constrained by Tully-Fisher
- v_{sys} — Galaxy systemic velocity
- $\cos(i)$ — Inclination
- ...

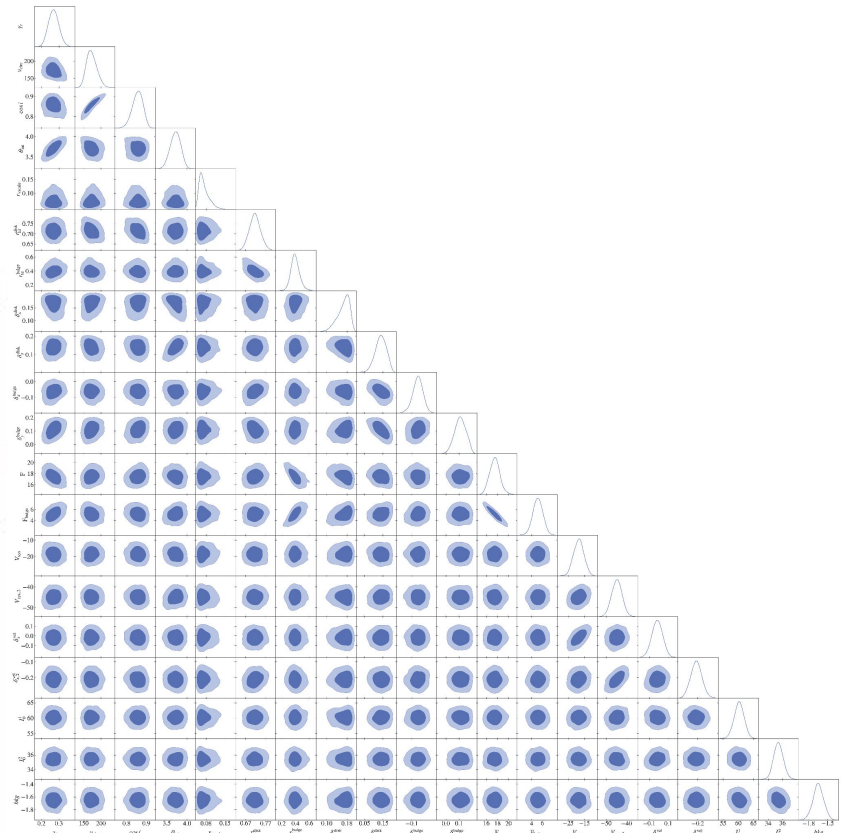
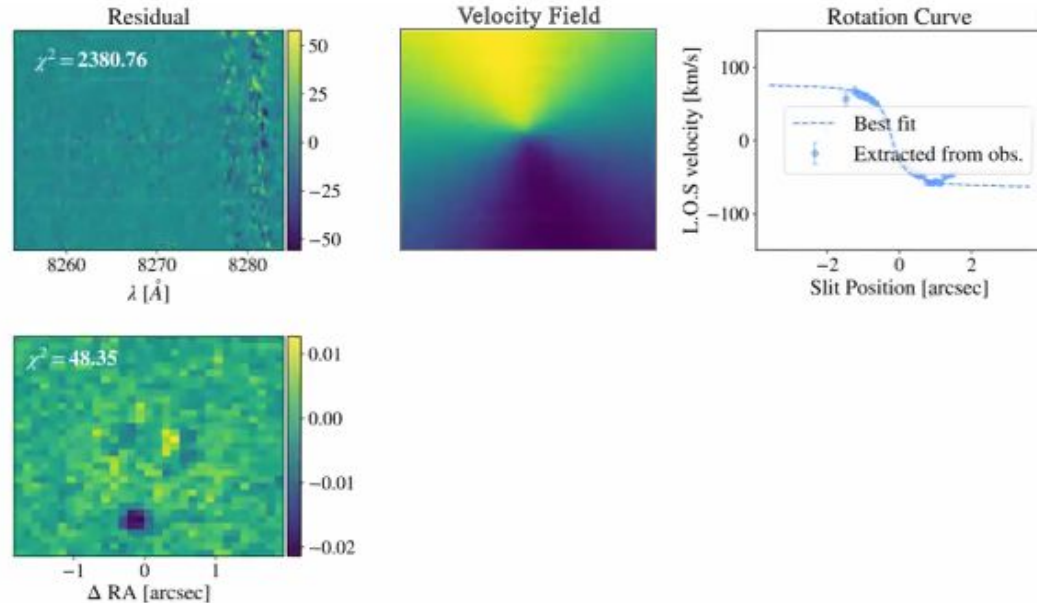


Courtesy of Pranjal R. S. (Arizona)

Results

Rotation Curves and Velocity Fields

KL measurement pipeline developed by Pranjal et al. (2023) and fit with the fast-forward model of 20 free parameters:

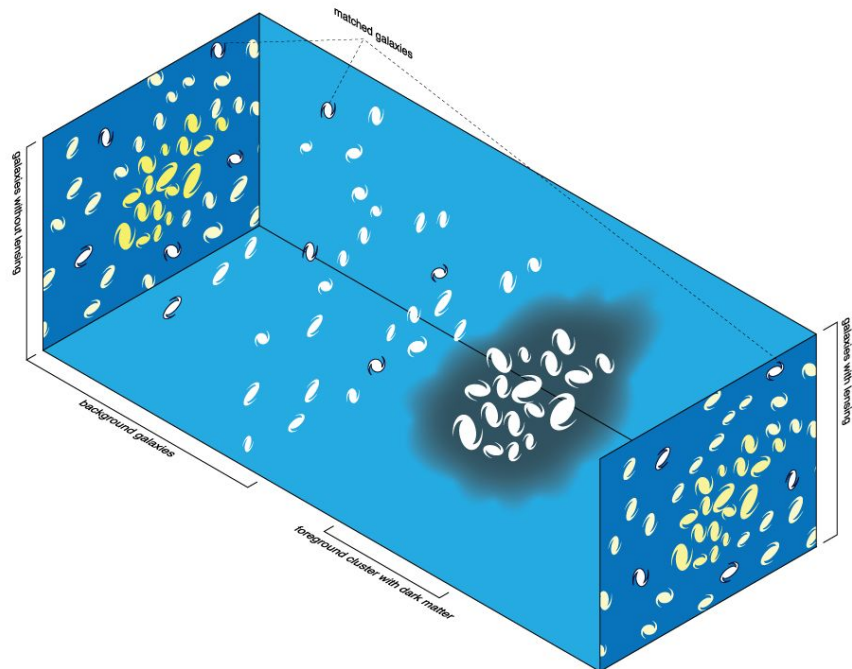


Courtesy of Pranjal R. S. (Arizona)

Results

Rotation Curves and Velocity Fields

- Background: $z > z_{\text{ci}} + 0.1$
- **149** rotation curves
- **105** rotation curves are background source galaxies



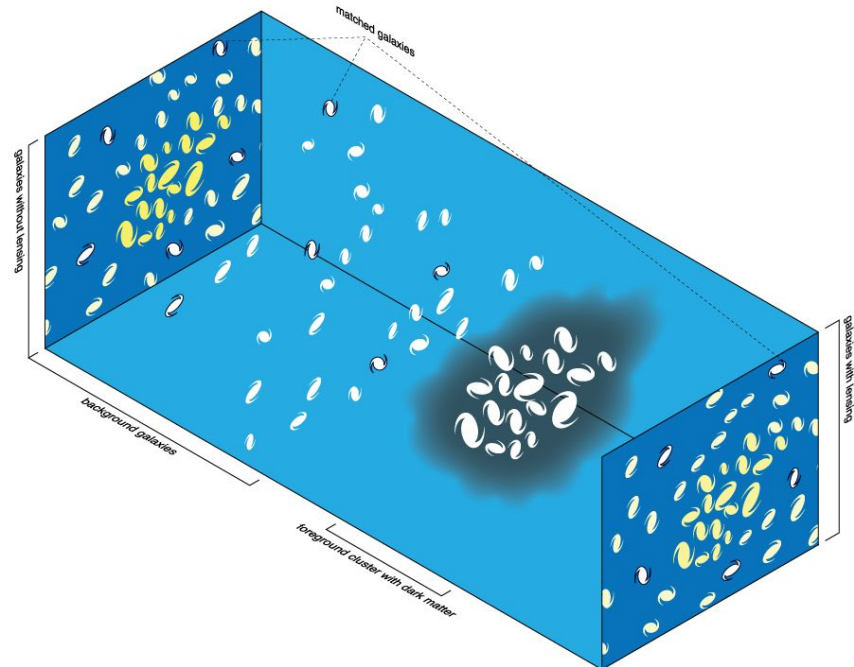
The effects of foreground galaxy cluster mass on background galaxy shapes

https://en.wikipedia.org/wiki/Weak_gravitational_lensing#Weak_lensing_by_clusters_of_galaxies

Results

Rotation Curves and Velocity Fields

- Background: $z > z_{\text{cl}} + 0.1$
- 149 rotation curves
- 105 rotation curves are background source galaxies
- Rotation curves whose redshifts $\mathbf{z \leq z_{\text{cl}} - 0.1}$ can be a key sample for training fittings
 - The galaxy is not weak-lensed
 - From photometry, it is exactly the intrinsic shape



The effects of foreground galaxy cluster mass on background galaxy shapes

https://en.wikipedia.org/wiki/Weak_gravitational_lensing#Weak_lensing_by_clusters_of_galaxies

Discussions and Future Works

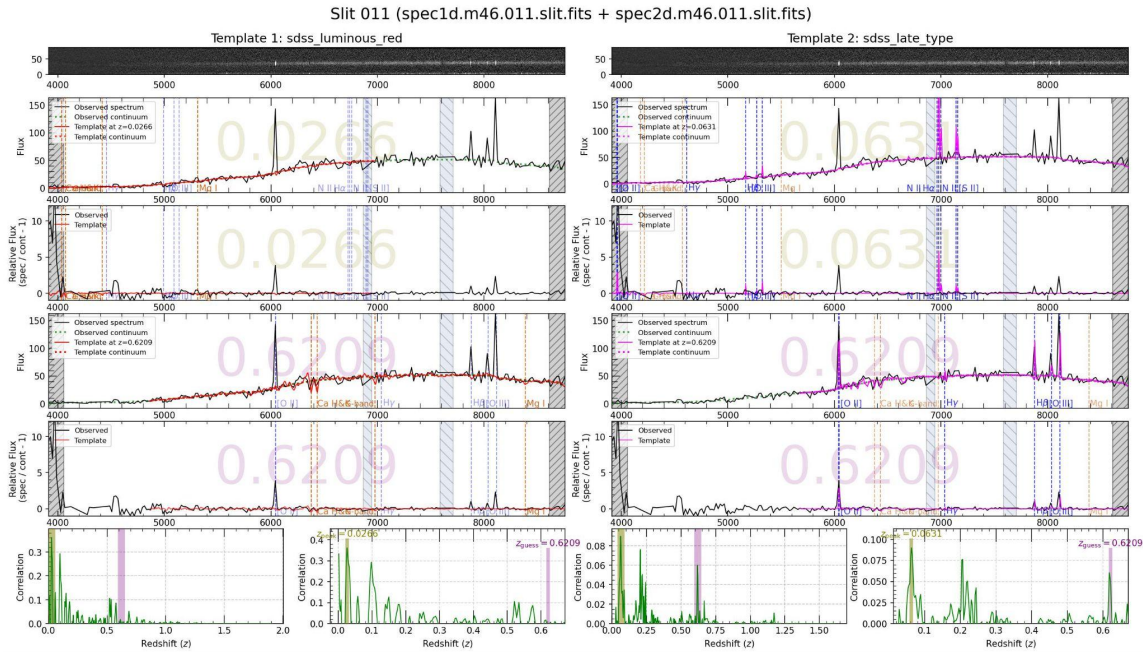
Redshift Pipeline

- The remaining 14 clusters and 40 masks in the cluster sample

Discussions and Future Works

Redshift Pipeline

- The remaining 14 clusters and 40 masks in the cluster sample
- Improve **FIREFLY** so that most spectroscopic redshifts can be assessed automatically
 - Manually-inspected confidence flag → cross-correlation parameter
 - Identify the significant emission lines such as [O II], [O III], and H β



Discussions and Future Works

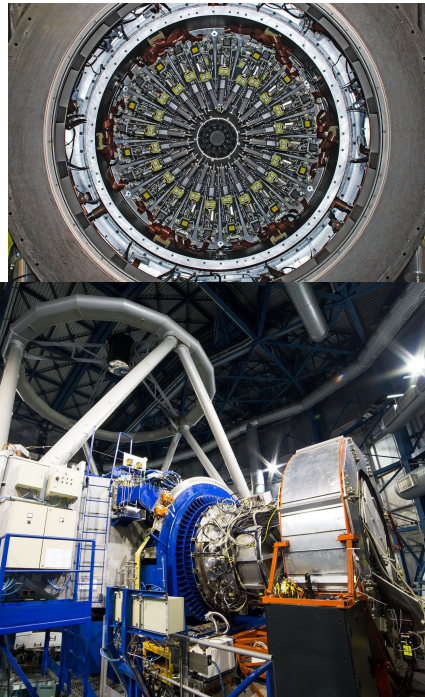
Shear Measurement

- Rotation curves give the magnitude and direction of the perpendicular shear component (γ_t).
- Cross-check with the previous and current generation weak lensing surveys.
- Cluster projected weak lensing mass map.

Discussions and Future Works

Future MOS Instruments

- VLT/KMOS (Sharples et al. 2013)
 - An integral-field MOS with 14×14 fibers
 - Wavelength-calibration-free data
 - Data cubes of x-pixels, y-pixels, and spectroscopic λ -pixels (spaxels)
 - Directly mapping the velocity fields
 - Up to 24 targets at one observation
- **9 clusters are with VLT/KMOS data**
- VLT/KMOS will show its potential in future KL analysis

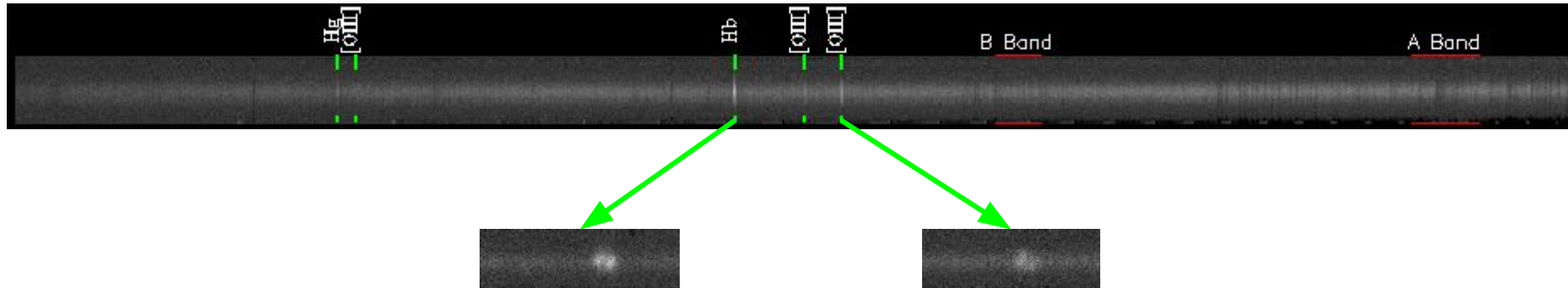


Discussions and Future Works

Discoveries of Active Galactic Nucleus

Emission line has **two distinct bright dots** separated for a few Å on the faint continuum

A2552 Slit 68: an irregular spiral galaxy (NASA/IPAC Extragalactic Database)



Conclusions

We reduced slit-spectroscopic data, discussed WL ideas, and showed rotation curves that can be fitted with resultant shears.

- A total of **443 secure spectroscopic redshifts** are measured by 1125 slits in 6 clusters.
- Rotation curves can solve for intrinsic shapes of galaxies, **without regarding if the galaxy is weak-lensed by a cluster**. They are also **valuable databases** for researchers who test and train for the rotation curve fitting by their models and algorithms.
- We find **149 rotation curves** that can solve for the weak lensing shear and reduce shape noise. They are also valuable databases for future KL studies.
- This paper utilizes and develops multiple pipelines by combining automatic template fittings and redshift measurements.
- Spectroscopic redshifts can be further analyzed for dynamical masses and cross-checking with weak-lensing masses.

References

- Allen, S. W.**, Evrard, A. E. & Mantz, A. B. (2011), Annual Review of A&A 49(1), 409–470.
<https://doi.org/10.1146/annurev-astro-081710-102514>
- Applegate, D. E.**, von der Linden, A., Kelly, P. L., et al. (2014), MNRAS 439(1), 48–72. <https://doi.org/10.1093/mnras/stt2129>
- Courteau, S.** (1997), AJ 114, 2402.
<https://ui.adsabs.harvard.edu/abs/1997AJ....114.2402C>
- Di, J.**, Egami, E., Wong, K. C., et al. (2023), arXiv e-prints p. arXiv:2312.02140.
<https://ui.adsabs.harvard.edu/abs/2023arXiv231202140D>
- DiGiorgio, B.**, Bundy, K., Westfall, K. B., et al. (2021), ApJ 922(2), 116.
<https://doi.org/10.3847/1538-4357/ac2572>
- Eifler, T.**, Miyatake, H., Krause, E., et al. (2021), MNRAS 507(2), 1746–1761.
<https://doi.org/10.1093/mnras/stab1762>
- Faber, S. M.**, Phillips, A. C., Kibrick, R. I., et al. (2003), Vol. 4841 of Society of Photo-Optical Instrumentation Engineers (SPIE) Conference Series, pp. 1657–1669.
<https://doi.org/10.1117/12.460346>
- Green, A. W.**, Glazebrook, K., McGregor, P. J., et al. (2014), MNRAS 437(2), 1070–1095. <https://doi.org/10.1093/mnras/stt1882>
- Gurri, P.**, Taylor, E. N. & Fluke, C. J. (2020), MNRAS 499(4), 4591–4604.
<https://doi.org/10.1093/mnras/staa2893>
- Gurri, P.**, Taylor, E. N. & Fluke, C. J. (2021), MNRAS 502(4), 5612–5621.
<https://doi.org/10.1093/mnras/stab423>
- Huff, E. M.**, Krause, E., Eifler, T., et al. (2013), arXiv e-prints p. arXiv:1311.1489. <https://doi.org/10.48550/arXiv.1311.1489>
- Kelly, P. L.**, von der Linden, A., Applegate, D. E., et al. (2014), MNRAS 439(1), 28–47. <https://doi.org/10.1093/mnras/stt1946>
- Mantz, A.**, Allen, S. W., Rapetti, D., et al. (2010a), MNRAS 406(3), 1759–1772. <https://doi.org/10.1111/j.1365-2966.2010.16992.x>
- Mantz, A.**, Allen, S. W., Ebeling, H., et al. (2010b), MNRAS 406(3), 1773–1795. <https://doi.org/10.1111/j.1365-2966.2010.16993.x>
- Masters, D.** & Capak, P. (2011), PASP 123(903), 638–644.
<http://iopscience.iop.org/article/10.1086/660023>
- Mroczkowski, T.**, Nagai, D., Basu, K., et al. (2019), Space Science Reviews 215(1), 17. <https://doi.org/10.1007/s11214-019-0581-2>
- Pranjali, R. S.**, Krause, E., Huang, H.-J., et al. (2023), MNRAS 524(3), 3324–3334. <https://doi.org/10.1093/mnras/stad2014>
- Reyes, R.**, Mandelbaum, R., Gunn, J. E., et al. (2011), MNRAS 417(3), 2347–2386. <https://doi.org/10.1111/j.1365-2966.2011.19415.x>
- Sharples, R.**, Bender, R., Agudo Berbel, A., et al. (2013), The Messenger 151, 21–23.
<https://ui.adsabs.harvard.edu/abs/2013Msngr.151...21S>
- Tanaka, M.**, Coupon, J., Hsieh, B.-C., et al. (2018), PASJ 70, S9.
<https://doi.org/10.1093/pasj/psx077>
- Tully, R. B.** & Fisher, J. R. (1977), A&A 54, 661–673.
<https://ui.adsabs.harvard.edu/abs/1977A&A....54..661T>
- von der Linden, A.**, Allen, M. T., Applegate, D. E., et al. (2014a), MNRAS 439(1), 2–27. <https://doi.org/10.1093/mnras/stt1945>
- von der Linden, A.**, Mantz, A., Allen, S. W., et al. (2014b), MNRAS 443(3), 1973–1978. <https://doi.org/10.1093/mnras/stu1423>
- Wittman, D.** & Self, M. (2021), ApJ 908(1), 34.
<https://doi.org/10.3847/1538-4357/abd548>
- Xu, J.**, Eifler, T., Huff, E., et al. (2023), MNRAS 519(2), 2535–2551.
<https://doi.org/10.1093/mnras/stac3685>



Spectroscopy Team of Anja's Group

Anja von der Linden, associate professor, Physics & Astronomy

Jiyun Di, Joined Sep 2022, 2nd-year MA student

Alden Beck, Joined Nov 2022, Nevis Labs, Columbia U

Aaron Burke, Joined Jan 2023, 1st-year MA student



Anja



Aaron

Jiyun

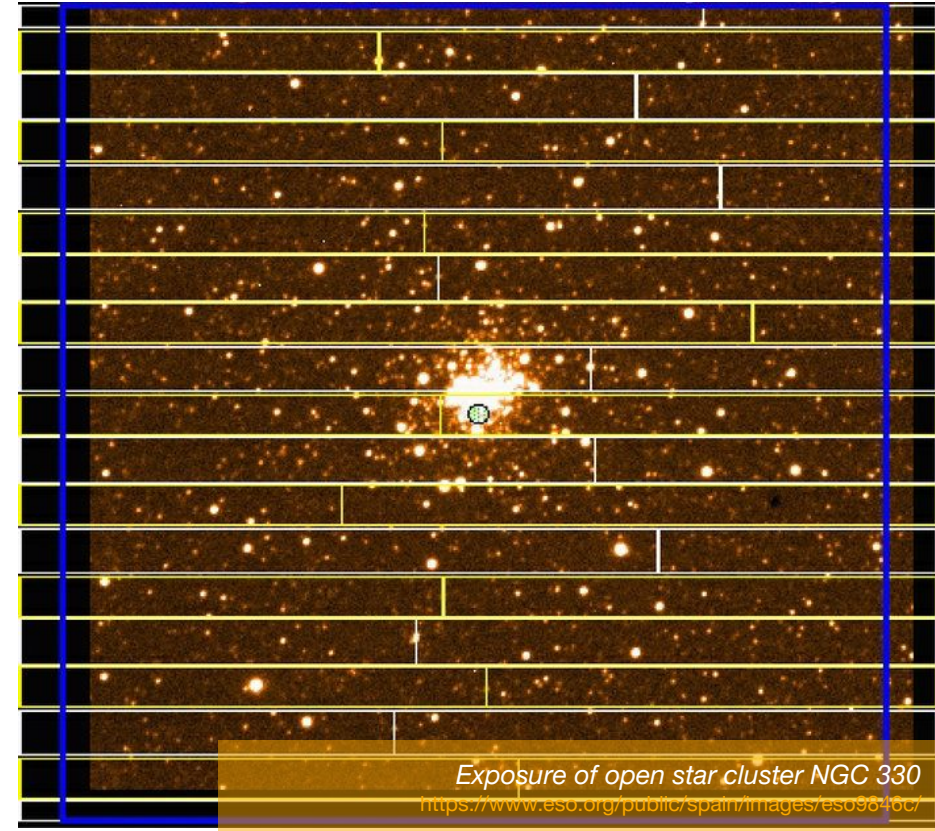
Alden

Appendix



Stony Brook
University

Galaxy Spectroscopy Multi-object Spectrograph (MOS)



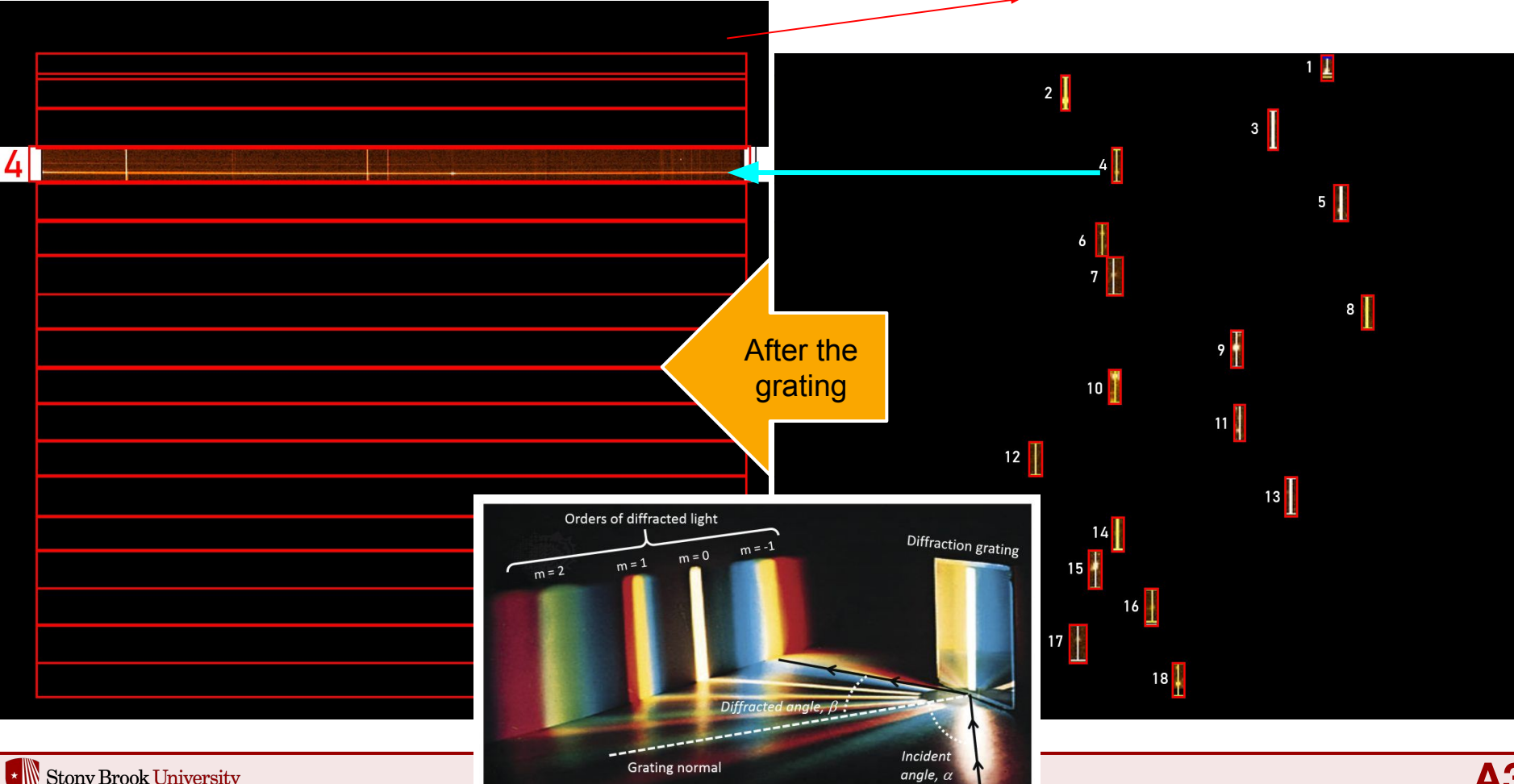
Exposure of open star cluster NGC 330

<https://www.eso.org/public/spain/images/eso9846c/>

Galaxy Spectroscopy Multi-object Spectrograph (MOS)

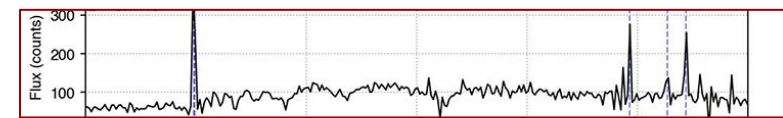
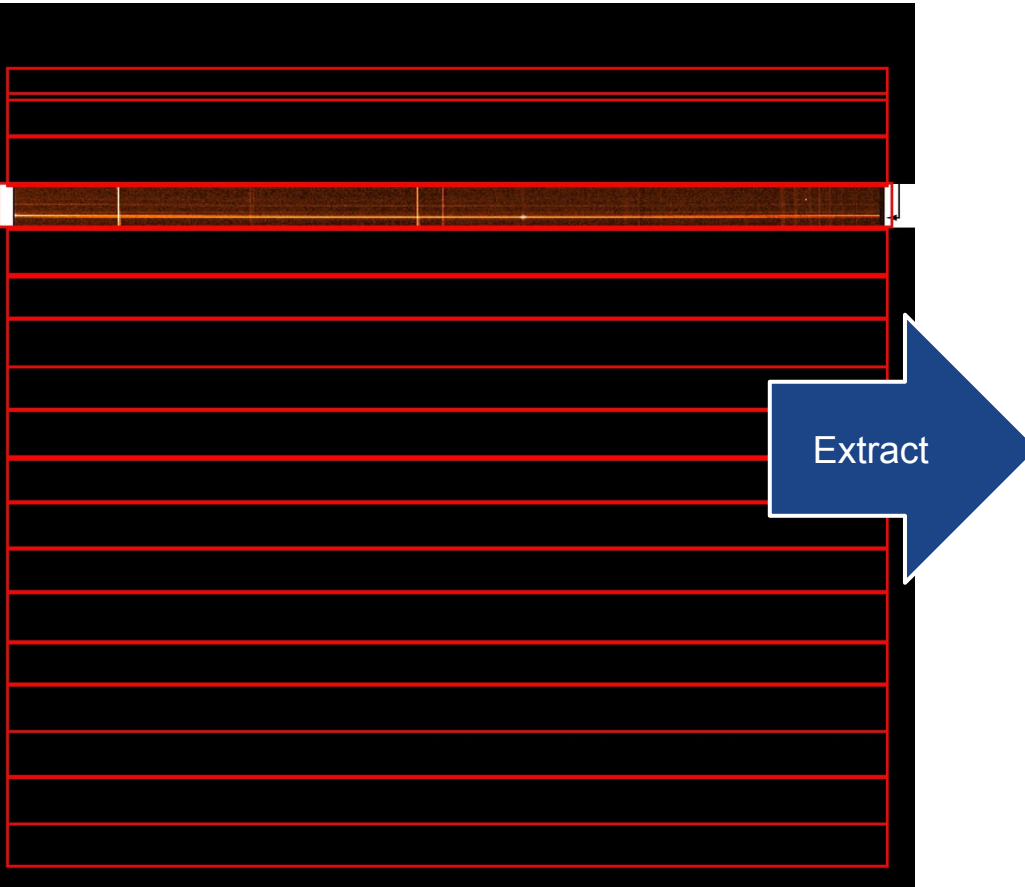


Galaxy Spectroscopy Multi-object Spectrograph (MOS) - 2D spectrum



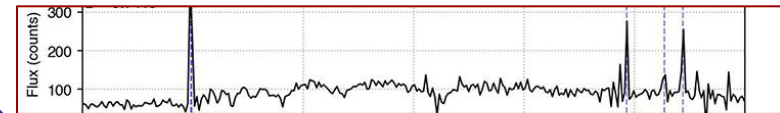
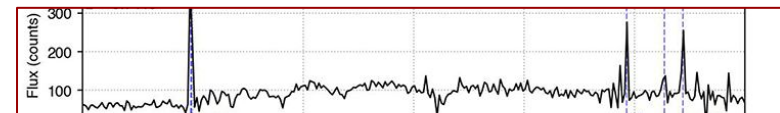
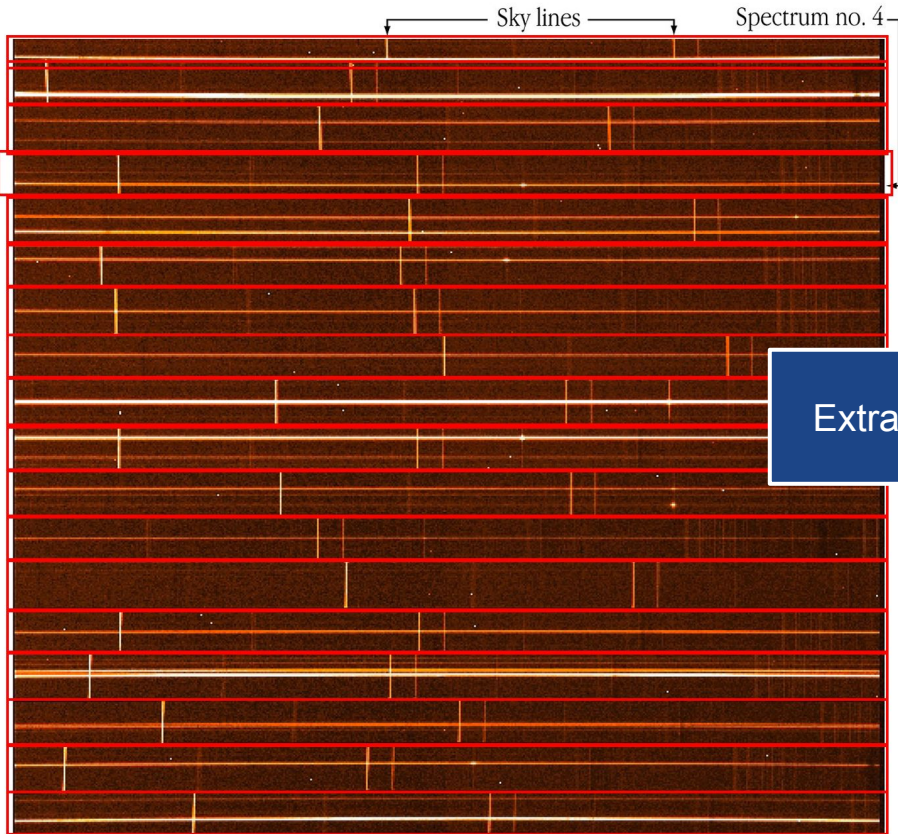
Galaxy Spectroscopy Multi-object Spectrograph (MOS) - 2D spectrum

4



Galaxy Spectroscopy Multi-object Spectrograph (MOS) - 2D & 1D spectra

4



...other slits

"Kinematic" information can be obtained now